

## COMPOSITION AND PARAGENESIS OF Na-, Nb- AND Zr-BEARING TITANITE FROM Khibina, Russia, AND CRYSTAL-STRUCTURE DATA FOR SYNTHETIC ANALOGUES

RUSLAN P. LIFEROVICH<sup>§</sup> AND ROGER H. MITCHELL

*Department of Geology, Lakehead University, 955 Oliver Road, Thunder Bay, Ontario P7B 5E1, Canada*

### ABSTRACT

We describe titanite with unusually high contents of Na, Nb, and Zr from a hydrothermal natrolite-rich vein cutting kalsilite-nepheline syenite at Mount Rasvumchorr, Khibina peralkaline complex, in the Kola Alkaline Province, Russia. This titanite is associated with astrophyllite, ceriobetafite, yttrobetafite, henrymeyerite, and banalsite. We recognize four generations of titanite: nearly stoichiometric titanite-I, titanite-II, containing up to 16.4 wt.% Nb<sub>2</sub>O<sub>5</sub> (0.25 *apfu* Nb) and 3.2% Na<sub>2</sub>O (0.21 *apfu* Na), titanite-III, with up to 9% ZrO<sub>2</sub> (0.15 *apfu* Zr) and zoned from 12.4 to 2.2% Nb<sub>2</sub>O<sub>5</sub>, and (Nb-Zr)-poor titanite-IV, with up to 3.6% Al<sub>2</sub>O<sub>3</sub> and 2.2% Fe<sub>2</sub>O<sub>3</sub>. In titanite-II, substitution of Nb at the octahedral site is accompanied by Na at the seven-fold site and, probably, by (F,OH)<sup>-</sup> and vacancies. A compositional analogue of titanite-III, and synthetic titanite containing 0.25 *apfu* Zr, similar to the most Zr-rich titanite known, have been prepared by standard ceramic techniques, and their crystal structure determined by Rietveld refinement of powder X-ray-diffraction patterns. The synthetic variants doped with Zr, or with Zr, Na, and Nb, adopt space group *A2/a*, and consist of distorted YO<sub>7</sub> polyhedra, XO<sub>6</sub> octahedra, and SiO<sub>4</sub> tetrahedra. The (Ca<sub>0.85</sub>Na<sub>0.15</sub>)(Ti<sub>0.70</sub>Zr<sub>0.15</sub>Nb<sub>0.15</sub>)OSiO<sub>4</sub> analogue of natural titanite from the Rasvumchorr zeolite vein contains the least-distorted coordination polyhedra. The polyhedra in Ca(Ti<sub>0.75</sub>Zr<sub>0.25</sub>)OSiO<sub>4</sub> are moderately distorted, and the most strongly distorted polyhedra are those in the CaTiOSiO<sub>4</sub> end-member.

**Keywords:** titanite, crystal structure, astrophyllite, henrymeyerite, banalsite, betafite, X-ray diffraction, Rietveld refinement, Mount Rasvumchorr, Khibina complex, Russia.

### SOMMAIRE

Nous décrivons un exemple de titanite avec des teneurs inhabituelles de Na, Nb, et Zr provenant d'un assemblage hydrothermal dans une veine recoupant une syénite à kalsilite + néphéline au mont Rasvumchorr, complexe hyperalkalin de Khibina, province alcaline de Kola, en Russie. La titanite est associée à l'astrophyllite, bétafite riche en Ce, bétafite riche en Y, henrymeyerite, et banalsite. Nous distinguons quatre générations de titanite: titanite-I, presque stœchiométrique, titanite-II, contenant jusqu'à 16.4% Nb<sub>2</sub>O<sub>5</sub> (0.25 atomes de Nb par formule unitaire, *apfu*) et 3.2% (poids) de Na<sub>2</sub>O (0.21 *apfu* Na), titanite-III, avec jusqu'à 9% ZrO<sub>2</sub> (0.15 *apfu* Zr) et zonée de 12.4 à 2.2% Nb<sub>2</sub>O<sub>5</sub>, et titanite-IV, à faible teneur en Nb et Zr, avec jusqu'à 3.6% de Al<sub>2</sub>O<sub>3</sub> et 2.2% de Fe<sub>2</sub>O<sub>3</sub>. Dans la titanite-II, la substitution du Nb au site octaédrique est accompagnée de Na au site à coordination sept, et tout probablement de (F,OH)<sup>-</sup> et de lacunes. Nous avons aussi préparé un analogue de la titanite-III et un échantillon avec 0.25 *apfu* Zr, semblable à la titanite la plus riche en Zr qui soit, par synthèse céramique standard, et nous en avons affiné la structure cristalline par méthode de Rietveld appliquée aux spectres de diffraction sur poudre. Les préparations synthétiques dopées avec Zr, ou avec Zr, Nb et Na, adoptent le groupe spatial *A2/a*, et contiennent des polyèdres difformes YO<sub>7</sub>, des octaèdres XO<sub>6</sub> et des tétraèdres SiO<sub>4</sub>. L'analogue synthétique de la titanite provenant de la veine du mont Rasvumchorr, de composition (Ca<sub>0.85</sub>Na<sub>0.15</sub>)(Ti<sub>0.70</sub>Zr<sub>0.15</sub>Nb<sub>0.15</sub>)OSiO<sub>4</sub>, possède les polyèdres de coordination les moins difformes. Les polyèdres de Ca(Ti<sub>0.75</sub>Zr<sub>0.25</sub>)OSiO<sub>4</sub> le sont davantage, et les plus fortement difformes sont ceux du pôle CaTiOSiO<sub>4</sub>.

(Traduit par la Rédaction)

**Mots-clés:** titanite, structure cristalline, astrophyllite, henrymeyerite, banalsite, bétafite, diffraction X, affinement de Rietveld, mont Rasvumchorr, complexe de Khibina, Russie.

<sup>§</sup> *Permanent address:* Geological Institute, Kola Science Center, Russian Academy of Sciences, 14 Fersmana Street, Apatity, 184200, Russia.

<sup>¶</sup> *E-mail address:* rmitchel@lakeheadu.ca

## INTRODUCTION

Titanite, ideally  $\text{CaTiOSiO}_4$ , has the general formula  $\text{XYOSiO}_4$ . It is a typical accessory orthosilicate in many alkaline rocks, and is common in nepheline syenites, some of which are large potentially economic deposits of low-grade titanium ore (Kulakov 1981). In titanite, a simple isovalent diadochy is commonly inferred to occur between  $\text{Zr}^{4+}$  and  $\text{Ti}^{4+}$  at the octahedral site, whereas the substitution of  $\text{Nb}^{5+}$  and  $\text{Ta}^{5+}$  is complex, and requires concomitant charge-balancing substitutions at the same or other sites.

In this paper, we present a description of the paragenesis and composition of the most (Na–Nb)-rich titanite yet discovered, together with an unusual Zr-rich titanite, occurring on Mount Rasvumchorr, in the Khibina peralkaline complex, Kola Alkaline Province, northwestern Russia. Titanite described by Černý *et al.* (1995) in a granite pegmatite contains considerably more total Ta plus Nb, but its composition is dominated by Ta. Recently, Chakhmouradian *et al.* (2003) described zirconian titanite from the Afrikanda ultramafic-alkaline complex, also in the Kola alkaline province, containing 15.3 wt.%  $\text{ZrO}_2$  (0.26 *apfu* Zr), this being the highest level of Zr yet reported. In this work, crystal-structure data are presented for (F,OH)-free synthetic titanite doped with (Na + Nb) or Zr (or both). Of these, one compound is similar to natural (Na–Nb–Zr)-rich titanite from the Rasvumchorr occurrence, and another is similar to the most strongly zirconian titanite known.

Titanite is one of a few  $\text{H}_2\text{O}$ -poor to anhydrous species that hosts a range of high field-strength elements (HFSE) in peralkaline rocks and their derivatives. This work is a further contribution to the mineralogy, geochemistry, and crystal chemistry of phases hosting incompatible elements in alkaline complexes, and is the first to characterize the mode of accommodation of Na, Nb, and Zr in the titanite structure.

## REVIEW OF THE STRUCTURAL FORMULA

The titanite structure is tolerant to a wide range of isomorphous substitution, according to Sahama (1946) and recent studies (*e.g.*, Oberti *et al.* 1991, Černý *et al.* 1995, Perseil & Smith 1995, Reguir *et al.* 1999, Chakhmouradian *et al.* 2003). The entry of the following elements in the structure has been documented (elements present in quantities  $\diamond 0.1$  atoms per formula unit [*apfu*] are shown in italics): i) the seven-fold site ( $^{\text{VII}}\text{X}$ ):  $\text{Ca}^{2+} \leftrightarrow \text{Na}^+$ ,  $\text{Ba}^{2+}$ ,  $\text{Mn}^{2+}$ ,  $\text{Pb}^{2+}$ ,  $\text{REE}^{3+}$  (the rare-earth elements), and  $\text{Y}^{3+}$ ; ii) the octahedral site ( $^{\text{VI}}\text{Y}$ ):  $\text{Ti}^{4+} \leftrightarrow \text{Fe}^{2+}$  (?),  $\text{Mg}^{2+}$  (?),  $\text{Al}^{3+}$ ,  $\text{Cr}^{3+}$ ,  $\text{Fe}^{3+}$ ,  $\text{Sc}^{3+}$ ,  $\text{Sr}^{4+}$ ,  $\text{Sn}^{4+}$ ,  $\text{Zr}^{4+}$ ,  $\text{Nb}^{5+}$ ,  $\text{Sb}^{5+}$ ,  $\text{Ta}^{5+}$ ,  $\text{V}^{5+}$ , and  $\text{U}^{6+}$ ; iii) the tetrahedral site ( $^{\text{IV}}\text{Si}$ ):  $\text{Si}^{4+} \leftrightarrow 4\text{H}^+$ ,  $\text{Al}^{3+}$ ,  $\text{Ti}^{4+}$ , and  $\text{P}^{5+}$ ; iv) the bridging anion site [only O(1)]:  $\text{O}(1)^{2-} \leftrightarrow \text{Cl}^-$ ,  $\text{F}^-$ , and  $\text{OH}^-$ .

There are no structural data on the incorporation in titanite of elements other than Sn,  $^{\text{VI}}\text{Si}$ , Al, the REE

(very limited range for La and Dy), F, and OH. Nevertheless, the structural characteristics of titanite hosting high-field-strength elements are of importance; for example, Ringwood *et al.* (1988) have proposed that titanite-structured ceramics can be used for the disposal of nuclear waste. Evaluation of this proposal requires comprehensive experimental work on the crystal chemistry of titanite, and in particular on the entry of the HFSE and fission products into the structure.

Natural occurrences of HFSE-rich varieties of titanite are listed in Table 1; they form only in parageneses related to highly evolved igneous systems. To date, Ta-rich titanite has been observed only from granitic pegmatites (Clark 1974, Černý *et al.* 1995). Niobian and zirconian varieties of titanite have been described from late derivatives related to diverse silica-undersaturated rocks, mainly peralkaline, and to carbonatite complexes (Chakhmouradian *et al.* 2003).

## OVERVIEW OF THE CRYSTAL STRUCTURE AND PHASE TRANSITIONS OF TITANITE

The structure of titanite (Fig. 1) is based on kinked chains of corner-linked  $\text{YO}_4(\text{O,F,OH})_2$  octahedra sharing the O(1) anions (the bridging oxygen) parallel to the crystallographic [100] axis. These octahedra are cross-linked by isolated  $\text{SiO}_4$  tetrahedra. Irregular  $\text{XO}_7$  polyhedra form interlacing chains sharing edges *via* couples of oxygen anions and extend down [101] (Speer & Gibbs 1976, Taylor & Brown 1976). The  $\text{YO}_6$  and  $\text{XO}_7$  chains are interconnected by shared edges. The titanite structure may be considered as a  $[\text{YOSiO}_4]^{2-}$  framework with irregular cavities enclosing X(Ca) cations in seven-fold coordination.

At ambient conditions, in the  $P2_1/a$  structure of  $\text{CaTiOSiO}_4$ , all  $^{\text{VI}}\text{Ti}^{4+}$  cations occur in off-center positions. The Ti cations are displaced coherently (in the same direction, *+**a*) within an individual  $\text{TiO}_6$  chain, but in opposite directions between neighboring chains, resulting in antiferroelectric interactions (Speer & Gibbs 1976, Kek *et al.* 1997). In this structure, there are two different Y–O(1) distances, resulting in regularly alternating long–short ... – Y – O(1) – Y – O(1') – ... distances along the chains of  $\text{YO}_6$  octahedra. According to Kunz & Brown (1994), the displacement of  $^{\text{VI}}\text{Y}(\text{Ti})$  cations “out of their otherwise regular octahedron coordination” is caused by an electronic second-order Jahn–Teller effect occurring around the octahedrally coordinated cations of this  $d^0$  transition metal. Kek *et al.* (1997) considered the ordering of Ca in the  $^{\text{VII}}\text{X}$  site as a trigger for the antiferroelectric displacement of the  $^{\text{VI}}\text{Y}(\text{Ti})$  cations in low-temperature  $\text{CaTiOSiO}_4$ .

The phase transitions known in titanite can be induced by either an increase in pressure, or temperature, or both (Kunz *et al.* 1996, 2000, Kek *et al.* 1997, Angel *et al.* 1999). They may also be induced by compositional changes involving the single  $\text{YO}_6$  site, or complex sub-

TABLE 1. OCCURRENCES OF HFSE-BEARING TITANITE

Locality	Geological setting	Composition
1. Craveggia, Piemonte, Italy	pegmatite	2.9 wt.% Nb <sub>2</sub> O <sub>5</sub> , 16.0 wt.% Ta <sub>2</sub> O <sub>5</sub>
2. Huron Claim, SE Manitoba	pegmatite, a vuggy Qtz–Ab zone	6.5 wt.% Nb <sub>2</sub> O <sub>5</sub> , 3.7 wt.% Ta <sub>2</sub> O <sub>5</sub>
3. Roccamonfina volcano, Rome, Italy	trachyandesitic xenolith in leucotrachytic tuffs	≤2.4 wt.% ZrO <sub>2</sub> , ≤0.6 wt.% Nb <sub>2</sub> O <sub>5</sub>
4. Ilomba, northern Malawi	foliated nepheline syenite	≤1.7 wt.% ZrO <sub>2</sub> , ≤11.1 wt.% Nb <sub>2</sub> O <sub>5</sub>
5. Mt. Bisson, British Columbia	granitic pegmatite "related to alkaline rocks"	≤5.7 wt.% Nb <sub>2</sub> O <sub>5</sub> , ≤3.5 wt.% ΣREE oxides
6. Šumperk–Maršíkov district, Hruby Jeseník Mts., Moravia	metamorphosed pegmatite (amphibolite facies)	≤9.5 wt.% Nb <sub>2</sub> O <sub>5</sub> , ≤21.53 wt.% Ta <sub>2</sub> O <sub>5</sub>
7. Oldoinyo Lengai, Tanzania	nepheline syenite xenolith in pyroclast	≤4.2 wt.% ZrO <sub>2</sub> , ≤1.5 wt.% Nb <sub>2</sub> O <sub>5</sub>
8. Pegmatite Peak, Bearpaw Mtns., Montana, USA	nepheline syenite pegmatite	≤6.4 wt.% Nb <sub>2</sub> O <sub>5</sub> , ≤2.9 wt.% Na <sub>2</sub> O
9. Tre Croci, Vico volcano, Italy	holocrystalline volcanic ejectum of alkali syenite	≤2.4 wt.% ZrO <sub>2</sub> , ~3.6 wt.% ΣREE <sub>2</sub> O <sub>3</sub>
10. Dara-i-Pioz, Tajikistan	quartz – albite – aegirine pegmatite	≤2.3 wt.% ZrO <sub>2</sub> , ≤1.7 wt.% Nb <sub>2</sub> O <sub>5</sub>
11. Afrikanda massif, Kola alkaline province, Russia	calcite – apatite – pyroxene pegmatite	≤15.3 wt.% ZrO <sub>2</sub> , ≤11.4 wt.% Nb <sub>2</sub> O <sub>5</sub>
12. Prairie Lake, Ontario	calciocarbonatite	≤6.8 wt.% ZrO <sub>2</sub> , ≤4.1 wt.% Nb <sub>2</sub> O <sub>5</sub>
13. Saxothuringian, Variscan orogen, Germany	lamprophyre	≤5.9 (9.8) wt.% ZrO <sub>2</sub>
14. Pilansberg peralkaline complex, South Africa	lujavrite subjected to autometamorphic alteration	≤5.3 wt.% ZrO <sub>2</sub> , ≤4.0 wt.% Nb <sub>2</sub> O <sub>5</sub>
15. Mt. Rasvumchorr, Khibina massif, Kola Province, Russia	zeolite vein related to kalsilite – nepheline syenite (rischorrite)	≤9.0 wt.% ZrO <sub>2</sub> , ≤16.2 wt.% Nb <sub>2</sub> O <sub>5</sub> , ≤3.2 wt.% Na <sub>2</sub> O

References: 1 Clark (1974), 2 Paul *et al.* (1981), 3 Gianetti & Luhr (1983), 4 Woolley *et al.* (1992), 5 Russell *et al.* (1994), 6 Černý *et al.* (1995), 7 Dawson *et al.* (1995), 8 Chakhmouradian & Mitchell (1999), 9 Della Ventura *et al.* (1999), 10 Reguir *et al.* (1999), 11, 12 Chakhmouradian *et al.* (2003), 13 Seifert & Kramer (2003), 14 Mitchell & Liferovich (in prep.), 15 this work.

stitutions involving the YO<sub>6</sub> + O(1) or XO<sub>7</sub> + YO<sub>6</sub> sites (Higgins & Ribbe 1976, Speer & Gibbs 1976, Troitzsch & Ellis 2002). The PT-driven transitions of the CaTiOSiO<sub>4</sub> end-member are stepwise and culminate in centering of the octahedrally coordinated atoms in the YO<sub>6</sub> polyhedra due to equalization of the Y–O(1) and Y–O(1') distances at  $P \diamond 3.5$  GPa or  $T > 825$  K (Kunz *et al.* 2000, Malcherek 2001), and in oscillations of the <sup>VII</sup>X cation between two positions (Kek *et al.* 1997). An intermediate non-quenchable transition between 496 and 825 K (Ghose *et al.* 1991, Van Heurk *et al.* 1991, Salje *et al.* 1993) results from loss of long-range order and creation of antiphase boundaries between O(1)–Y–O(1') dipoles, leaving domains of  $P2_1/a$  symmetry on the unit-cell scale, but an overall, pseudocentered  $A2/a$  symmetry on a long-range scale (Taylor & Brown 1976, Higgins & Ribbe 1976, Speer & Gibbs 1976, Kunz *et al.* 1996, Hughes *et al.* 1997, Troitzsch *et al.* 1999). The position of the <sup>VII</sup>X cation is split in this intermediate phase (Kek *et al.* 1997). Troitzsch & Ellis (2002) labeled the low-temperature phase with space group  $P2_1/a$   $\alpha$ -titanite, the intermediate  $A2/a$  phase as  $\beta$ -titanite, and the high-PT phase with "true  $A2/a$  symmetry" as  $\gamma$ -titanite. A further temperature-driven phase transition is possible above 1150 K (Chrosch *et al.*

1997). Conventionally, the  $\alpha \rightarrow \beta$  transformation is called the  $P2_1/a$  to  $A2/a$  phase transition, bearing in mind that it probably does not strictly represent the entire  $P2_1/a \rightarrow A2/a$  transformation (Troitzsch & Ellis 2002).

In pure CaTiOSiO<sub>4</sub>, different types of polyhedra have different responses to high pressure and temperature. The SiO<sub>4</sub> tetrahedra show a strong angular distortion with only minor change in bond lengths, whereas the polymerized CaO<sub>7</sub> polyhedra are significantly distorted and the TiO<sub>6</sub> octahedra rotate rigidly (Kunz *et al.* 2000).

Compositionally driven phase-transitions in titanite are similar to those driven by high pressure or high temperature. At ambient conditions, entry of <sup>VII</sup>REE<sup>3+</sup> stabilizes the  $\beta$  polymorph more readily than substitutions at the octahedral site;  $\beta$ -titanite can be stabilized with as little as 5 mol.% <sup>VII</sup>Dy<sup>3+</sup> coupled with 5 mol.% charge-balancing <sup>VI</sup>Al<sup>3+</sup> (Hughes *et al.* 1997). In the case of substitutions at the octahedral site balanced by an equal amount of F<sup>–</sup> at the O(1) site, the  $\beta$  polymorph dimorph becomes stable where <sup>VI</sup>Al<sup>3+</sup> exceeds 9 mol.% (Troitzsch *et al.* 1999), and a further  $\beta \rightarrow \gamma$  type of transformation might be expected for a more Al-rich titanite.

PARAGENESIS OF Na-, Nb-  
AND Zr-BEARING TITANITE

Rarely encountered variants of titanite enriched in Na, Nb, and Zr occur in a natrolite vein cutting leucite-normative kalsilite-nepheline rischorrite at Mount Rasvumchorr, Khibina peralkaline complex, Kola Province, northwestern Russia. This vein was recognized 25 years ago (Men'shikov *et al.* 1979) as an occurrence of titanite, a priderite-group barian titanate now established as henrymeyerite (Mitchell *et al.* 2000), leucophanite, titanian "hydrogarnet", kassite, and other rare mineral species. The rischorritic host-rock differs from other poikilitic feldspathoid-bearing syenites of the Khibina complex in having high K contents (8.21 to 15.4 wt.% K<sub>2</sub>O), a molar K:Na ratio of up to 2.6, and by the presence of normative leucite, kalsilite and wadeite (Arzamastsev 1994). X-ray diffractometry coupled with compositional data show that the rock contains up to 15–20 vol.% kalsilite (Kozyreva *et al.* 1990). The genesis of this ultrapotassic kalsilite-nepheline syenite is not understood. It might originate either by intense potassium metasomatism of precursor syenites or the formation of a K-rich residual liquid derived by fractional crystallization of nepheline. Removal of the latter from the magma chamber as a crystal mush might give rise to the urtite and juvite series of sodic nepheline syenites (Ivanova & Arzamastsev 1985). Such ultrapotassic

rischorrite has been mapped as a few linear zones 0.5–1.2 km in width and up to several km in length within the main urtite – juvite – rischorrite sequence (Kozyreva *et al.* 1990), which forms the hanging wall of the giant apatite-nepheline Rasvumchorr deposit in the central part of the Khibina complex.

Unusual HFSE-rich variants of titanite occur as granular aggregates and wedge-shaped single crystals ranging from a submillimetric size up to 4 cm in length and embedded in columnar natrolite. The core of the titanite aggregates is composed of an early honey-yellow to brown titanite (henceforth, titanite-I), which is euhedral but shows some corrosion at the contacts with the later generations of minerals. Titanite-I is invariably mantled by greenish to grey titanite with a high reflectance. Small grains of the latest titanite cannot be distinguished by eye from the natrolite matrix as they are water-clear and colorless. The outermost zones of the titanite aggregates, and some areas along cracks, are of a milky white color, with a dull luster. All generations of titanite observed in the Rasvumchorr occurrence exhibit widely variable composition (see below). Aggregates are intimately intergrown (Figs. 2a, b), and do not provide homogeneous material suitable for crystal-structure study.

The titanite-bearing paragenesis consists of large single crystals of bronze-brown astrophyllite, which are commonly split at the edges into a series of parallel

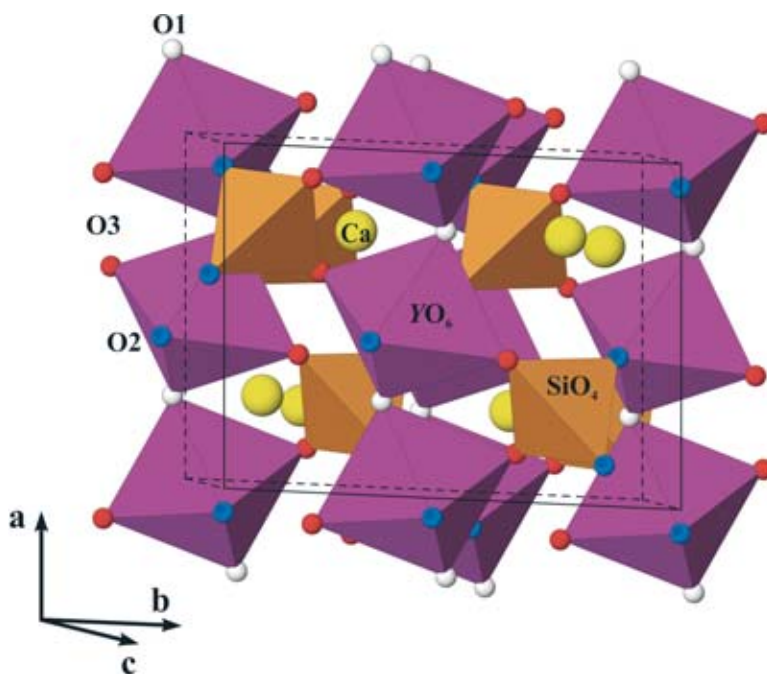


FIG. 1. The crystal structure of titanite.

fibrous individuals growing into the natrolite matrix, and subjected to replacement by kassite. Blocky orthoclase is strongly corroded and replaced by natrolite. Large euhedral flattened crystals of milky to translucent leucophanite up to 12 cm in length are coated by an enamel-like mixture of unidentified products of alteration. Wadeite occurs as tiny subhedral inclusions in

titanite-I. Henrymeyerite forms lustrous euhedral crystals 0.05–1 mm in length (Fig. 2a), and is commonly embedded in single crystals of water-clear titanite (a zirconian variety, *i.e.*, titanite-III). At the deuteric stage, henrymeyerite was altered and replaced by rutile. Betafite appears as concentrically zoned radiating spherulites up to 2 mm in diameter. It appears primarily

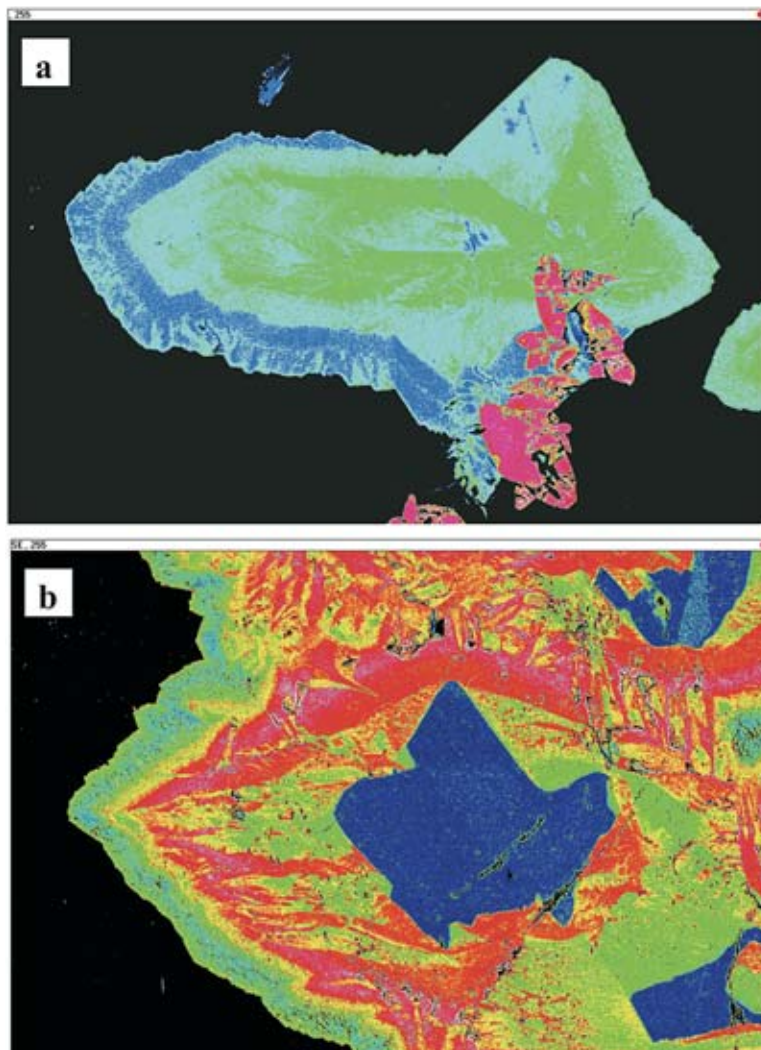


FIG. 2. False-color back-scattered-electron images showing the patterns of zoning in titanite-II (sodic niobian titanite, red-to-pink discontinuous zones and druses) and titanite-III (zirconian niobian, green-to-yellow anhedral) from Mount Rasvumchorr, Khibina. Titanite-I appears as blue euhedral cores; bluish to green margins consist of titanite-IV (aluminous ferrous variety). The black matrix is natrolite; the smaller red euhedral crystals associated with titanite-III (upper figure) consist of henrymeyerite. The width of the field of view is 0.6 mm in the upper figure, and 1.2 mm in the bottom figure.

in contact with titanite aggregates with no evidence of corrosion or replacement. Textural relationships show the earliest generation of betafite to have formed prior to the late generations of titanite. Banalsite forms single anhedral grains up to 0.3 mm in length that are not visually distinguishable from the zeolite matrix. The banalsite grains are poikilitic and contain abundant inclusions of natrolite. Anhedral pyrrhotite and chalcopyrite, mostly altered and replaced by a mixture of Fe–Mn oxides, occur near to the contact with the wallrock syenite. The natrolite vein was affected by late faulting along the axial zone and contacts, and was injected by hydrothermal solutions. This resulted in the fragmentation, alteration, replacement and cementation of all primary minerals, including titanite.

#### ANALYTICAL METHODS

All mineral compositions were determined by energy-dispersion X-ray Spectrometry (EDS) using a JEOL JSM–5900 scanning electron microscope (SEM) equipped with a Link ISIS 300 analytical system incorporating a Super ATW Element Detector (133 eV FWHM MnK). Raw EDS spectra were acquired for 130 s (live time) with an accelerating voltage of 20 kV, and beam current of 0.475 nA monitored on a Ni standard. The spectra were processed with the LINK ISIS–SEMQUANT software package, with full ZAF corrections applied. The following well-characterized mineral and synthetic standards were used: jadeite (Na), loparite (Ce, La, Pr, Nd), lueshite (Nb), orthoclase (K), corundum (Al), benitoite (Ba), ilmenite (Fe, Ti), hematite (Fe), periclase (Mg), zircon (Zr), wollastonite (Ca), metallic Mn (Mn), Ta (Ta), silicate glass standard DJ–35 (Si), synthetic YF<sub>3</sub> (Y, F), and SrTiO<sub>3</sub> (Sr). A multi-element standard for the REE was used, as it provides more accurate data than single-REE standards with EDS spectrum-stripping techniques. However, peak profiles used for the analytical lines were obtained using individual REE fluoride standards. The accuracy of the EDS method was cross-checked by wavelength-dispersion electron-microprobe analysis (WDS–EMPA) using an automated CAMECA SX–50 instrument (University of Manitoba) following methods described by Mitchell & Vladykin (1993). In addition, the accuracy of analytical results was checked every 1–1.5 hour on well-analyzed minerals such as lueshite, perovskite, loparite, eudialyte, benitoite, villiaumite and natrolite, studied in several laboratories by WDS–EMPA.

Special care was taken to avoid inclusions of niobian and zirconian phases in the samples of titanite analyzed. Inclusions larger than 0.5–0.1 μm were not detected by back-scattered-electron (BSE) imagery. Because of the sodic composition of Nb-rich titanite and its synthetic analogue, and low totals of cations in some natural samples of titanite, care was taken to minimize any possible volatilization of Na during analyses by employing raster scanning and by reducing counting periods. Re-

producibility (within analytical errors) of the compositions of the Na-rich titanite using the above approach demonstrates the compositional features of such titanite to be real. The reliability of the Na results was cross-checked by analyzing natrolite adjacent to the titanite every 1–1.5 hours. Stoichiometric compositions were obtained for this sodic zeolite, leaving no doubt that the data on Na content of the titanite are reliable.

Variants of titanite rich in high field-strength elements have been synthesised by solid-state ceramic techniques from stoichiometric amounts of TiO<sub>2</sub>, Nb<sub>2</sub>O<sub>5</sub>, ZrO<sub>2</sub>, CaSiO<sub>3</sub>, and Na<sub>2</sub>CO<sub>3</sub> (Alfa Aesar Chemical Co., high-purity grade); the latter component was taken with a 5 mol.% excess to compensate for volatilization of Na. The reagents, dried at 120°C for several days, were mixed, ground in an agate mortar under acetone, and calcined in air for 24 h at 1000°C. After regrinding, the samples were pelletized, and then heated in air for 96 h, with grinding every 48 h. The temperature of the synthesis was individually tailored for each sample using duplicates for the determination of solidi at ambient pressure (with a step of 20°C). The solid-state (subsolvus) synthesis of all the samples was performed at temperatures 10–20°C below their solidi.

Step-scanned powder X-ray-diffraction (XRD) patterns of the synthetic products were obtained at room temperature using a Philips 3710 diffractometer ( $T = 20^\circ\text{C}$ , radiation  $\text{CuK}\alpha$ ,  $2\theta$  range  $9^\circ$ – $145^\circ$ ,  $2\theta$  step  $0.02^\circ$ ; time per step 2 s) with an APD powder-diffraction software. In addition, high-resolution XRD patterns were obtained in the  $2\theta$  range  $31.7^\circ$ – $33.4^\circ$  ( $\Delta 2\theta$  step  $0.005^\circ$ ; time per step 30 s).

The XRD patterns were inspected using the Bruker AXS EVA diagnostic software. Data were further analyzed by Rietveld methods using the TOPAS 2.1 software (Kern & Coelho 1998). Refined variables included: zero corrections, scaling factors, cell dimensions, positional coordinates of the atoms, preferred orientation corrections, and isotropic thermal parameters (the latter were kept equal for all oxygen anions).

The ATOMS-6.0 software package (Dowty 1999) was used to determine interaxial angles describing the distortion of coordination polyhedra and selected bond-lengths. We employed the IVTON program (Balić-Žunić & Vicković 1996) to characterize the coordination spheres of the cations, volumes of coordination polyhedra, and displacements of cations from the centers of coordination polyhedra.

#### COMPOSITIONAL VARIATIONS IN THE Khibina TITANITE

At least four consecutive generations of titanite, differing greatly in composition and forming discontinuous concentric zones, which are corroded and cemented by later generations of titanite, are best distinguished using BSE imagery (Fig. 2). Representative compositions of titanite are given in Table 2. The compositions

in this table are numbered from the center toward the margin of the complex aggregates of titanite analyzed.

Figure 3 shows a comparison of the titanite compositions from the Mount Rasvumchorr vein with previously published data on HFSE-rich varieties of titanite in terms of substitutions at the octahedral site. As the titanite variants studied in this work do not contain detectable Ta, the sum Nb + Ta actually refers only to Nb in our data. It is evident that  $^{VI}Zr$  and  $^{VI}Nb$  do not substitute for  $^{VI}Ti$  to the same extent in the different generations of titanite (Fig. 3a, see below), and the valence-excess substitution,  $^{VI}Nb^{5+} \rightarrow ^{VI}Ti^{4+}$ , is followed by a valence-deficient scheme,  $^{VI}(Al,Fe)_3^{3+} \rightarrow ^{VI}Ti^{4+}$  from early to late generations of titanite (Fig. 3b).

A noteworthy feature of the Rasvumchorr titanite is its low REE content, which is much below of that found in counterparts from other peralkaline syenites and alkaline rocks (*e.g.*, Russell *et al.* 1994, Della Ventura *et al.* 1999, Chakhmouradian & Mitchell 1999). Of the rare-earth elements, only Ce was detected, with the highest concentrations (0.6–1.0 wt.%  $Ce_2O_3$ ) found in

niobian titanite associated with the early generation of betafite (see below).

Titanite-I occurs as a euhedral core within the titanite aggregates or as zoned crystals (shown in blue on Fig. 2b). It contains very few minor constituents, among which only Nb reaches detectable levels ( $\leq 0.8$  wt.%  $Nb_2O_5$ , #1, 2 in Table 2; Figs. 3a, b). Titanite-I is slightly corroded, and invasive embayments are filled with later generations of titanite transitional from HFSE-rich to aluminous compositions (see below).

BSE images show that the (Na–Nb)-rich titanite (titanite-II) forms fragmented drusy aggregates mantling euhedral titanite-I crystals (Fig. 2b, orange to red and pink colors). The titanite-II fragments are not displaced, and are cemented by the same or later generations of titanite. Titanite-II is strongly enriched in Nb (up to 16.4 wt.%  $Nb_2O_5$ , or 0.25 *apfu* Nb, see Table 2, #5), and Na (up to 3.2 wt.%  $Na_2O$ , or 0.21 *apfu* Na). Titanite-II demonstrates a continuous enrichment in Zr outward in the concentrically zoned aggregates, which are 75–120  $\mu m$  in thickness. Over this distance, Zr increases from 1.2 to 3.9 wt.%  $ZrO_2$  (Table 2, #4 to 7). The abundance of

TABLE 2. REPRESENTATIVE COMPOSITIONS OF TITANITE FROM MOUNT RASVUMCHORR, Khibina, Russia

	I		II					III			Transitional		IV	
	1	2	3	4	5	6	7	8	9	10	11	12	13	14
$Na_2O$ wt.%	0.56	0.70	1.87	2.31	3.00	3.18	2.06	1.74	1.32	1.45	0.61	0.77	0.16	0.14
CaO	28.12	27.73	25.51	23.74	22.62	22.47	22.56	24.36	23.72	24.83	26.18	26.03	27.22	27.19
$Y_2O_3$	n.d.	n.d.	-	-	n.d.	n.d.	n.d.	n.d.	n.d.	n.d.	n.d.	n.d.	0.29	0.12
$Ce_2O_3$	n.d.	n.d.	-	-	n.d.	n.d.	0.95	n.d.	n.d.	0.41	n.d.	n.d.	n.d.	0.14
$Fe_2O_3^a$	0.42	0.22	1.57	0.96	0.76	1.01	1.00	0.71	1.06	0.73	1.52	1.79	1.92	1.81
$Al_2O_3$	n.d.	n.d.	n.d.	0.83	0.31	0.23	0.29	0.20	0.73	0.81	0.99	0.99	3.49	3.55
$TiO_2$	40.49	40.46	34.91	32.78	27.58	28.38	27.20	26.22	25.71	28.78	31.78	29.62	30.53	30.79
$Nb_2O_5$	0.80	0.44	6.19	7.71	16.42	15.51	13.13	12.40	8.69	6.25	2.11	6.67	2.42	2.23
$ZrO_2$	n.d.	n.d.	n.d.	1.24	1.42	1.38	3.91	6.99	8.86	7.61	7.42	4.49	1.81	1.83
$SiO_2$	29.99	30.47	30.98	31.79	28.89	29.63	28.59	28.44	29.48	30.51	30.24	29.20	30.63	30.64
Total	100.38	100.02	101.03	101.36	101.0	101.69	99.68	101.06	99.57	101.38	100.85	99.56	98.47	98.72
Na <i>apfu</i>	0.035	0.044	0.118	0.146	0.197	0.206	0.139	0.116	0.089	0.094	0.039	0.051	0.010	0.009
Ca	0.979	0.965	0.890	0.828	0.819	0.804	0.839	0.896	0.880	0.889	0.932	0.945	0.964	0.967
Y	-	-	-	-	-	-	-	-	-	0.005	-	-	0.005	0.002
Ce	-	-	-	-	-	-	0.012	-	-	-	-	-	-	0.002
Ti	0.989	0.989	0.854	0.83	0.701	0.713	0.709	0.677	0.669	0.723	0.794	0.754	0.759	0.764
Zr	-	-	-	0.020	0.023	0.022	0.066	0.117	0.149	0.124	0.120	0.074	0.029	0.029
Nb	0.012	0.006	0.091	0.113	0.251	0.234	0.206	0.192	0.136	0.094	0.032	0.102	0.036	0.033
$Fe^{3+}$	0.010	0.005	0.038	0.024	0.019	0.023	0.026	0.018	0.028	0.018	0.038	0.046	0.048	0.045
Al	-	-	-	0.032	0.012	0.009	0.012	0.008	0.030	0.032	0.039	0.040	0.136	0.138
Si	0.974	0.990	1.008	1.032	0.977	0.989	0.992	0.976	1.020	1.020	1.005	0.989	1.012	1.011

The structural formulae are calculated on the basis of three cations. <sup>a</sup> Total Fe given as  $Fe_2O_3$ ; n.d.: not determined. The generation of titanite is given as a Roman numeral. Compositions: 1, 2: primary euhedral crystal, core and periphery, respectively; 3–13 concentric zones representative of consecutive generations of late titanite; 14: the latest, outermost zone.

trivalent cations (considering all Fe as  $^{VI}Fe^{3+}$ ) alone does not match the imbalance resulting from the heterovalent  $^{VI}Nb^{5+} \rightarrow ^{VI}Ti^{4+}$  substitution (Fig. 3b). A combination of  $Na^+$  plus trivalent cations in the most niobian titanite is very close to the abundance of  $^{VI}Nb^{5+}$  (Fig. 4), and indicates that the substitutions occur at both the seven-fold and octahedral sites:  $^{VII}Na^+ + 2 ^{VI}Nb^{5+} + ^{VI}(Al,Fe)^{3+} \rightarrow ^{VII}Ca^{2+} + 3 ^{VI}Ti^{4+}$ , with some inferred replacement of O(1) by monovalent anions ( $F^-$  and  $OH^-$ ) or vacancies.

A plot of Nb (+Ta) versus  $(Al,Fe)^{3+} + Na^+$  (Fig. 4) demonstrates the complex compositional characteristics of titanite-II. The earliest, inner parts of this titanite, which have the most Nb-rich compositions, plot on, or in the vicinity of, the 1:1 substitution line involving both  $^{VII}Na^+$  and  $^{VI}(Al,Fe)^{3+}$  as charge-balancing cations (trend along line 2–2). Moving from core to margin of the niobian titanite-II aggregates, within the more-or-

less uniform areas, we found some intermediate and marginal zones with compositions plotting below the 1:1 substitution line. This part of the titanite-II composition field shows a trend nearly parallel to the 1:1 substitution line (trend along line 2'–2' on Fig. 4). The fact that the proportion of  $Na^+$  greatly exceeds that of  $(Al,Fe)^{3+}$  in titanite-II (Table 2, #3–7) is responsible for this trend. As this is not an analytical artefact, this trend implies the involvement of equivalent quantities of monovalent anions ( $F^-$ ,  $OH^-$ ) at the O(1) site to maintain charge balance (e.g., Isetti & Penco 1968, Mongiorgi & Riva di Sanseverino 1968, Černý & Riva di Sanseverino 1972, Paul *et al.* 1981, Russell *et al.* 1994, Della Ventura *et al.* 1999), or the presence of some vacancies at the  $^{VII}X$  site (Table 2, #4). This observation suggests that the substitution scheme  $^{VII}Na^+ + (F,OH)^- \leftrightarrow ^{VII}Ca^{2+} + O(1)^{2-}$  does occur, as assumed for Na–Nb-rich titanite described from hydrothermally altered nepheline syenite

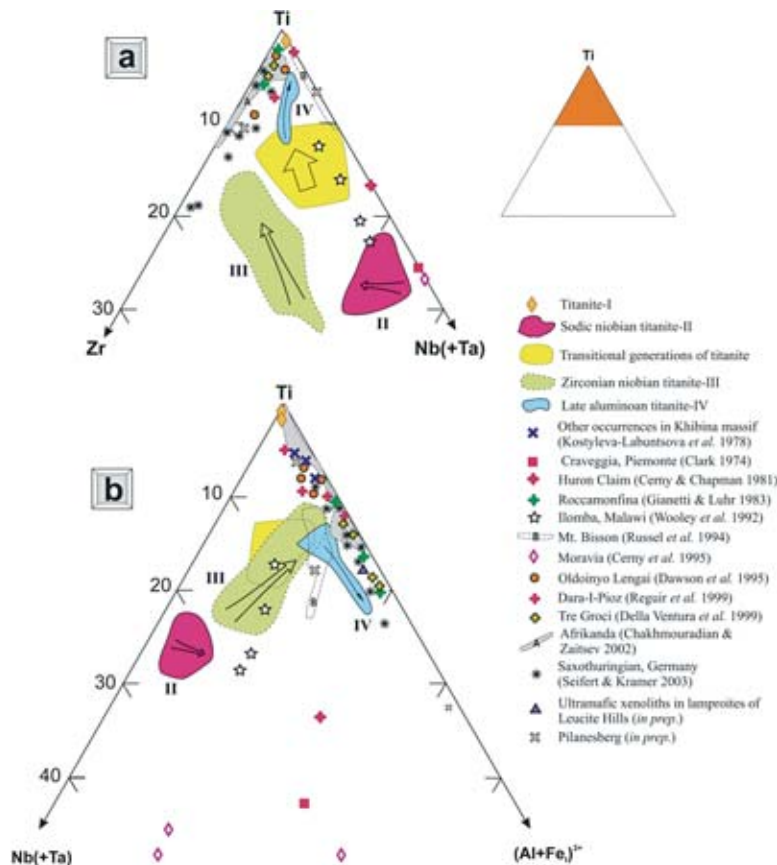


FIG. 3. Triangular plots of a) Zr – Nb – Ti and b) (Nb+Ta) – Ti – (Al+Fe) of titanite compositions (apfu). The arrows indicate compositional trends; Roman numerals indicate the generations of titanite. The HFSE-poor compositions are not plotted in a).

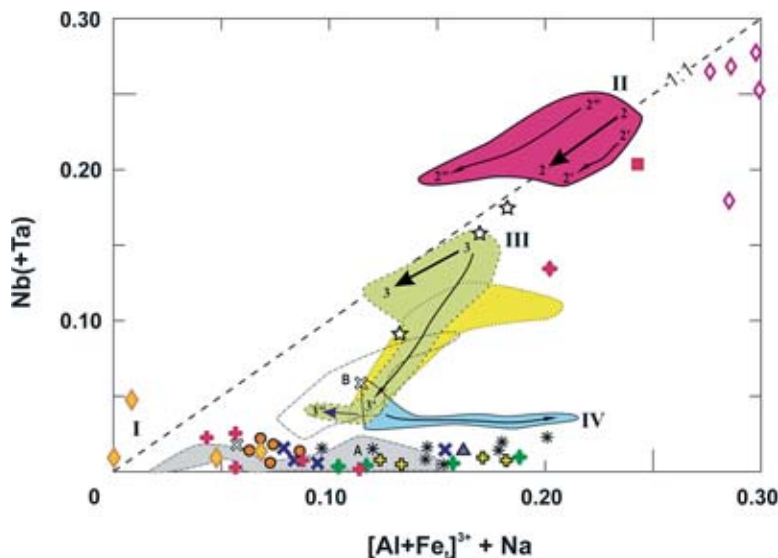


FIG. 4. Plot of titanite compositions (*apfu*) in terms of the effect of possible schemes involving entry of Nb at the  $^{VI}Y$  site of the titanite structure *via* the double substitutions  $^{VII}Na^{+} + ^{VI}Nb^{5+} \leftrightarrow ^{VII}Ca^{2+} + ^{VI}Ti^{4+}$  and  $^{VI}(Al,Fe)^{3+} + ^{VI}Nb^{5+} \leftrightarrow 2 ^{VI}Ti^{4+}$ . For the legend, see Figure 3. Roman numerals indicate generations of titanite; trends within the given compositional fields are marked in Arabic numerals and shown by arrows (see text for details).

pegmatite at Pegmatite Peak, Bearpaw Mountains, Montana (Chakhmouradian & Mitchell 1999). Unfortunately, the morphology of the titanite aggregates, which consist of complexly intergrown variants of diverse composition, does not provide homogeneous representative samples of the “Na-excess” titanite-II for the study of its anionic composition by infrared spectroscopy.

In contrast, marginal zones of fragmented titanite-II aggregates and some inner areas along the cracks show compositions plotting above the 1:1 substitution line (Fig. 4, trend along 2”–2” line), *i.e.*, a deficiency of “balancing cations” as compared to  $^{VI}Nb^{5+}$ . The discontinuous morphology of these zones, resulting from numerous cracks cemented with titanite of the same or later generation(s), suggests that some inner areas of titanite-II druses might have experienced alteration during the complex fragmentation-cementation processes, resulting in an imbalance between  $Nb^{5+}$  and  $(Al,Fe)^{3+} + Na^{+}$ , most probably, by removal of Na.

There is a compositional gap between the outermost, Zr-rich zones of the titanite-II, and the next generation (Figs. 2b, 3, 4), which evolved from zirconian niobian to zirconian titanite. The latter is considered as titanite-III (green and yellow on Fig. 2a and Fig. 2b, respectively), and appears as concentric zones, mantling and cementing titanite-II aggregates (Fig. 2b), or as concentric zones in the cores of single crystals embedded in natrolite (Fig. 2a).

In common with titanite-II, the compositions of earliest titanite-III plot on, or in the vicinity of, the 1:1 substitution line on Figure 4 (trend along the line 3–3) and evolve along this line as the content of Nb and “balancing cations” decreases coherently. Evolution along the 1:1 substitution line is typical for most areas of titanite-III. There is another trend within the compositional field of the titanite-III, observed at the margins of aggregates (line 3–3’), caused by a stepwise depletion in Nb and some enrichment in  $(Al,Fe)^{3+}$ , resulting in a steeper slope than the 1:1 substitution line (Fig. 4). The outermost parts of the titanite-III have compositions trending toward the 1:1 substitution line (short trend 3’–3”). We interpret this observation to reflect the possible increasing role of charge-balancing  $(F,OH)^{-}$  anions or vacancies, as proposed above for the altered areas of titanite-II.

The latest generation, titanite-IV, distinguished on a compositional and morphological basis, is considerably enriched in Al, contains relatively low amounts of Zr and Nb, and is “depleted” in Na relative to all other generations (Table 2, #13, 14; shown in shades of blue and green on Figs. 2a, b). In this titanite, Zr and Nb are not abundant (0.03–0.04 *apfu*), whereas the total  $^{VI}(Al + Fe)^{3+}$  content reaches 0.20 *apfu* ( $Al \gg Fe$ ) $^{3+}$ . Where the concentration of the trivalent cations in titanite-IV is not matched by that of  $^{VII}Na^{+}$ , we infer that the sub-

stitution scheme becomes  ${}^{\text{VI}}(\text{Al} + \text{Fe})^{3+} + (\text{F}, \text{OH})^{-} \rightarrow {}^{\text{VI}}\text{Ti}^{4+} + \text{O}(\text{I})^{2-}$  (Della Ventura *et al.* 1999, and references therein), as typically observed in titanite occurring in low-temperature metamorphic rocks.

There is a transitional variant (perhaps variants) of titanite, mantling, and probably replacing the primary HFSE-rich generations. This type is moderately enriched in HFSE and shows wide variations in cationic compositions (patchy green to yellowish areas in Fig. 2b). Development of this transitional titanite within the aggregates of titanite (Fig. 2b) implies that it formed during fracturing and partial replacement of aggregates of the precursor HFSE-rich titanite. The latter agrees with compositional characteristics, shown in Figure 3. This titanite forms a diffuse transitional compositional field between fields of titanite-III and titanite-IV.

#### MINERALS ASSOCIATED WITH NA-, NB- AND ZR-BEARING TITANITE

*Henrymeyerite* is abundant in the paragenesis with titanite-II. The mineral has a composition almost identical to that of the holotype (Mitchell *et al.* 2000). Crystallochemical characteristics, calculated upon the basis of 16 atoms of oxygen (Table 3, #1), show the mineral to be a heptatitanate with 6.8 *apfu* Ti and 0.99 *apfu* Fe<sup>2+</sup>. Of the minor constituents, the most abundant are Nb<sup>5+</sup> (0.11 *apfu*) and Ca<sup>2+</sup> (0.07 *apfu*); Na and Ce are less abundant.

*Astrophyllite* in the Rasvumchorr natrolite vein shows moderate  ${}^{\text{VI}}\text{Fe}^{2+} \leftrightarrow {}^{\text{VI}}(\text{Mn} + \text{Mg})^{2+}$  substitutions involving the <sup>VI</sup>C sheet-forming sites, coupled with less intense  $\text{K}^{+} \leftrightarrow \text{Na}^{+}$  substitution at the <sup>X-XIII</sup>A site (Table 3, #2, 3; for site designation, see Piilonen *et al.* 2003). At nearly constant Fe<sup>3+</sup> content, the Mn:Mg ratio evolves from 1.28 in center of the astrophyllite crystals to 0.95 at their margin. The Na/(Na + K) value does not change appreciably from core to margin. There is no systematic enrichment of astrophyllite in Zr, Nb, Na, and Mn as described from other undersaturated rocks (Piilonen *et al.* 2003). Zirconium slightly decreases, whereas niobium slightly increases from the center to the margin of the crystals. Fluorine is observed, but its concentration was not established quantitatively because of overlap of *FK*α with *L*α lines of transition metals in the EDS spectra.

*Banalsite*, discovered in the Rasvumchorr zeolite vein hosting the Na-, Nb- and Zr-rich titanite, is the first occurrence of this rare species in the Khibina complex. The banalsite has nearly the pure end-member composition, and contains no more than 0.7 wt.% SrO (Table 3, #4).

Rock-forming columnar *natrolite*, comprising about 90–95 vol.% of the vein, is of near-ideal composition. The mean of 12 compositions is given in Table 3, #5).

There are two generations of *pyrochlore-group minerals* differing in composition (Table 4). These occur in the radiating cores and rims of the same spherulitic ag-

gregates. According to the classification scheme proposed by Hogarth (1989), an earlier generation, associated with titanite-II, is regarded as lanthanian “ceriobetafite” (Ti >> 2Nb, both Ce and La > 0.2 *apfu*, Ce > La). The quotation marks signify that “ceriobetafite” is not approved by the CNMMN, IMA. The mineral contains considerable Y and Nd (Table 4, #1).

The second generation of pyrochlore is ceroan ytrobetafite. This rare species has not previously been observed in the Khibina and Lovozero peralkaline complexes. Ytrobetafite (betafite-II) coexists with the zirconian titanite (titanite-III). The mineral has Nb < 2Ti, contains 0.29 *apfu* Y, 0.04 *apfu* Zr, and shows some depletion in REE in marginal zones at nearly constant Ca (Table 4, #2, 3). Both generations of betafite are represented by A-site-deficient Si-bearing varieties and contain insignificant Ba, Sr, Fe, Mn and Al. Tantalum, U and Th are below the detection limit. The deficiency at the A site increases from 1.04 *apfu* in the “ceriobetafite” to 1.17 *apfu* in the latest ytrobetafite, in

TABLE 3. COMPOSITIONS OF MINERALS ASSOCIATED WITH TITANITE IN ZEOLITE VEIN FROM MOUNT RASVUMCHORR, RUSSIA

Wt.%	1	2	3	4	5
Na <sub>2</sub> O wt.%	0.24	2.91	3.14	9.46	15.73
K <sub>2</sub> O	0.12	7.25	7.28	n.d.	0.24
CaO	0.47	1.78	2.19	n.d.	n.d.
SrO	n.d.	n.d.	n.d.	0.75	n.d.
BaO	n.d.	0.23	n.d.	23.45	n.d.
MgO	n.d.	3.28	2.81	n.d.	n.d.
MnO	0.14	4.52	5.19	n.d.	n.d.
FeO*	9.00	27.41	26.45	n.d.	n.d.
Al <sub>2</sub> O <sub>3</sub>	n.d.	n.d.	n.d.	31.45	26.29
Ce <sub>2</sub> O <sub>3</sub>	0.85	n.d.	n.d.	n.d.	n.d.
TiO <sub>2</sub>	69.16	12.44	12.22	n.d.	n.d.
Nb <sub>2</sub> O <sub>5</sub>	1.82	0.40	0.74	n.d.	n.d.
ZrO <sub>2</sub>	b.d.	0.72	0.27	n.d.	n.d.
SiO <sub>2</sub>	n.d.	37.53	38.31	36.21	45.63
F	b.d.	2.42	2.28	n.d.	n.d.
O=F	-	1.02	0.95	-	-
Total	99.45	100.10	99.80	101.33	87.89
Na <i>apfu</i>	0.061	1.188	1.272	2.001	1.990
Ca	0.066	0.401	0.490	-	-
Sr	-	-	-	0.047	-
Ba	-	0.019	-	1.001	-
Mg	-	1.029	0.875	-	-
Mn	0.016	0.806	0.918	-	-
Fe <sup>2+</sup>	0.985	4.825	4.621	-	-
K	0.020	1.947	1.940	-	0.020
Al	-	0.020	-	4.039	2.022
Ce	0.041	-	-	-	-
Ti	6.803	1.969	1.920	-	-
Nb	0.108	0.038	0.070	-	-
Zr	-	0.074	0.028	-	-
Si	-	7.899	7.983	3.946	2.977
F	-	1.611	1.487	-	-

Column headings: 1 henrymeyerite entrapped in titanite-II (Fig. 2); 2 and 3 astrophyllite, center and margin of a crystal; 4 banalsite embedded in natrolite, in association with titanite-III; 5 natrolite. Basis for calculation of structural formulae: in columns 1 and 4: 16 atoms of oxygen, in column 5: 10 atoms of oxygen, and in columns 2 and 3: total of cations in D and T sites of the astrophyllite structure (Piilonen *et al.* 2003) equal to 10.

parallel with depletion in REE (from *ca.* 0.59 to 0.15 *apfu*, respectively). Yttrobetafite (betafite-II) contains much less F, which is, probably, replaced by OH<sup>-</sup>. The structural role of silicon in the pyrochlore structure is still uncertain (Chakhmouradian & Mitchell 2002), and its occurrence in betafite in amounts up to 0.08 *apfu* Si might be due to "amorphous" (finely dispersed) structurally unbound silica (Voloshin *et al.* 1989). As a result of the high A-site deficiency, the total positive charge of cations hosted in the A and B sites is less than 11.20<sup>+</sup> (10.94<sup>+</sup> in early lanthanian "ceriobetafite"), as opposed to the theoretical value of 13.0<sup>+</sup>. This significant deficiency implies that both cations at the A site and anions in the Y site (O and F+OH) were removed, probably as a result of deuteric leaching. The extent of this alteration of the Rasvumchorr betafite is comparable to that described recently for uranoan pyrochlore from unweathered murmanite lujavrite in the Lovozero peralkaline complex (Chakhmouradian & Mitchell 2002), but differs from A-site-deficient pyrochlore-group minerals from unweathered lujavrite in the subvolcanic Pilansberg peralkaline complex, South Africa (unpubl. data).

The reason for the strong depletion of hydrothermal solutions in Ce and La, and their enrichment in Y, which occurred between the stage of crystallization of "ceriobetafite" and that of yttrobetafite, is unclear. This process might be similar to the fractionation of REE and Y in peralkaline rocks during their evolution toward exotic hyperagpaitic derivatives (Khomyakov 1995,

Pekov 2001). Commonly, fractionation of lanthanides in the Khibina, Lovozero, and Pilansberg peralkaline agpaitic complexes results in exotic La mineralization consisting of rare silicates (nordite group, cerite, *etc.*), carbonates (bastnäsite, ancylite, among others), and phosphates (belovite, vitusite, rhabdophanite). Yttrium mineralization appears in the most evolved pegmatites in the Lovozero and Khibina complexes (Khomyakov 1995, Pekov 2001), and is associated with the latest sodic (hyperagpaitic) hydrothermal and epithermal parageneses. The close association of HFSE-rich titanite with yttrium mineralization in the Rasvumchorr zeolite vein indicates that these rare variants of titanite formed from the most evolved low-temperature hydrothermal solutions derived from the nepheline syenitic magma.

#### SYNTHETIC ANALOGUES OF Zr- AND (Na-Nb-Zr)-RICH TITANITE

The designations, empirical formulae, temperature of synthesis and crystallochemical characteristics of the synthetic analogues of Zr- and (Na-Nb-Zr)-rich titanite prepared are given in Table 5. Positional and thermal parameters of the TnZr<sub>25</sub> and RSV<sub>Syn</sub> samples are listed in Table 6. Selected bond-lengths in the coordination polyhedra are given in Table 7. The pure titanite end-member, CaTiOSiO<sub>4</sub> (Tn<sub>Syn</sub>), was synthesized as a reference material to assess the accuracy of the refinement procedure. The unit-cell dimensions and crystallochemical parameters of this titanite agree well with synchrotron-derived data published by Kek *et al.* (1997) for synthetic CaTiOSiO<sub>4</sub> (Tables 5, 7).

#### RIETVELD REFINEMENTS

Figure 5 illustrates high-resolution X-ray-diffraction patterns for all titanite samples synthesized over the range of 31.7–33.4° 2θ. Diffraction peaks in this region are observed only in the pattern obtained for CaTiOSiO<sub>4</sub>, and can be attributed to the 221 and 222 reflections in space group *P2<sub>1</sub>/a*. These *k + l = odd* reflections are not permitted in space group *A2/a* (*e.g.*, Kunz *et al.* 1996). Thus we interpret the absence of the diffraction peaks in the patterns of the Zr- and (Na-Nb-Zr)-bearing titanite (TnZr<sub>25</sub> and RSV<sub>Syn</sub>) to imply that entry of Zr into the titanite structure alone or in combination with Na plus Nb at ambient conditions results in a phase transition from *P2<sub>1</sub>/a* to an *A2/a* structure.

We used the atom coordinates of Kek *et al.* (1997) as a starting model for Rietveld refinement of the *P2<sub>1</sub>/a*-structured CaTiOSiO<sub>4</sub> end member, and those given by Oberti *et al.* (1991) for *A2/a*-structured Zr- and (Na-Nb-Zr)-rich variants of titanite. Figures 6a and 6b show portions of the Rietveld refinement plot for the TnZr<sub>25</sub> and RSV<sub>Syn</sub> samples, respectively. All the structure refinements were performed with data for the full 9–145° 2θ range).

TABLE 4. COMPOSITIONS OF PYROCHLORE-GROUP MINERALS ASSOCIATED WITH TITANITE IN ZEOLITE VEIN, MOUNT RASVUMCHORR, Khibina, RUSSIA

	1	2	3		1	2	3
Na <sub>2</sub> O wt.%	n.d.	n.d.	0.17	Na <i>apfu</i>	-	-	0.02
CaO	3.12	6.15	6.72	Ca	0.181	0.351	0.378
SrO	1.14	0.46	n.d.	Sr	0.036	0.014	-
BaO	0.85	1.31	n.d.	Ba	0.020	0.027	-
MnO	0.31	n.d.	n.d.	Mn	0.014	-	-
Fe <sub>2</sub> O <sub>3</sub>	0.92	0.81	0.73	Fe <sup>3+</sup>	0.042	0.036	0.029
Y <sub>2</sub> O <sub>3</sub>	3.78	10.12	10.20	Y	0.109	0.287	0.285
La <sub>2</sub> O <sub>3</sub>	10.88	2.95	2.12	La	0.217	0.058	0.041
Ce <sub>2</sub> O <sub>3</sub>	14.03	4.87	3.57	Ce	0.278	0.095	0.069
Pr <sub>2</sub> O <sub>3</sub>	n.d.	n.d.	0.38	Pr	-	-	0.007
Nd <sub>2</sub> O <sub>3</sub>	4.70	4.28	1.92	Nd	0.091	0.081	0.036
Al <sub>2</sub> O <sub>3</sub>	0.62	0.74	0.31	Al	0.040	0.046	0.019
TiO <sub>2</sub>	35.32	21.88	21.65	Ti	1.438	0.876	0.854
Nb <sub>2</sub> O <sub>5</sub>	16.69	38.54	41.30	Nb	0.409	0.928	0.980
ZrO <sub>2</sub>	n.d.	1.51	1.60	Zr	-	0.039	0.041
ThO <sub>2</sub>	n.d.	n.d.	n.d.	Th	-	-	-
SiO <sub>2</sub>	1.33	1.39	1.46	Si	0.072	0.074	0.077
F	2.92	1.45	1.05	F	0.500	0.244	0.174
-O=F	1.23	0.61	0.44				
Total	96.61	95.85	92.06	Σ <sub>B</sub>	2	2	2

total iron as Fe<sub>2</sub>O<sub>3</sub> (*apfu* in Fe<sup>3+</sup>). The structural formulae were calculated on the basis of a sum of 2 atoms in the B site (*i.e.*, Ti, Nb, *etc.*); n.d.: not determined. Samples: 1: "ceriobetafite" core (porous); 2, 3: "yttrobetafite", intermediate and outermost zone, respectively.

TABLE 5. RESULTS OF RIETVELD REFINEMENT AND CRYSTAL-STRUCTURE PARAMETERS FOR SYNTHETIC TITANITE

	KekTtn*	Ttn <sub>Syn</sub>	TtnZr <sub>25</sub>	RSV <sub>Syn</sub>		KekTtn	Ttn <sub>Syn</sub>	TtnZr <sub>25</sub>	RSV <sub>Syn</sub>
<i>a</i> , Å	7.0697(3)	7.0599(1)	7.1136(2)	7.1276(1)	<X-O>, Å	2.457(1)	2.463(12)	2.469(6)	2.484(6)
<i>b</i> , Å	8.7223(4)	8.7156(1)	8.7724(2)	8.7541(2)	<i>V</i> <sub>XO7</sub> , Å <sup>3</sup>	19.662(1)	19.887(20)	20.088(10)	20.538(10)
<i>c</i> , Å	6.5654(4)	6.5597(1)	6.5987(2)	6.6031(2)	Δ <sub>7</sub>	2.42	2.90	2.20	1.94
β, °	113.853(4)	113.797(1)	113.581(2)	113.847(2)	<i>v</i> <sub>7</sub>	0.162	0.157	0.157	0.154
<i>V</i> , Å <sup>3</sup>	370.27(1)	369.30(1)	377.40(2)	376.83(2)	<Y-O>, Å	1.959(1)	1.966(14)	2.018(4)	1.992(4)
<i>R</i> <sub>wp</sub> , %		11.50	6.71	8.21	<i>V</i> <sub>YO6</sub> , Å <sup>3</sup>	9.969(1)	10.095(15)	10.902(5)	10.507(5)
<i>R</i> <sub>Bragg</sub> , %		3.01	2.09	2.89	<i>d</i> <sub>Y</sub>	0.113	0.060	-	-
GoF		1.31	1.20	1.34	∂ <sub>xY</sub>	0.015	0.009	-	-
DW		1.26	1.46	1.21	∂ <sub>yY</sub>	0.004	0.000	-	-
					∂ <sub>zY</sub>	0.0	0.003	-	-
					Δ <sub>6</sub>	2.20	2.35	2.24	1.73
Ti-O(1)-Ti, °	141.5	143.2	141.6	143.6	<i>v</i> <sub>6</sub>	0.002	0.004	0.004	0.003
Si-O(2)-Ti, °	144.6	142.5	140.1	141.4	δ <sub>6</sub>	9.40	2.56	2.19	1.20
Si-O(3)-Ti, °	138.4	139.5	125.0	127.1	<Si-O>, Å	1.647(1)	1.622(14)	1.626(6)	1.616(6)
Si-O(4)-Ti, °	128.7	130.1			<i>V</i> <sub>SiO4</sub> , Å <sup>3</sup>	2.283(1)	2.177(12)	2.194(5)	2.152(5)
Si-O(5)-Ti, °	125.1	128.1			Δ <sub>4</sub>	0.002	0.19	0.14	0.04
					<i>v</i> <sub>4</sub>	0.005	0.007	0.009	0.006
					δ <sub>4</sub>	12.66	17.24	16.60	13.76

\* Synchrotron radiation data for CaTiOSiO<sub>4</sub> (Kek *et al.* 1997); Ttn<sub>Syn</sub>: titanite end-member, CaTiOSiO<sub>4</sub> (this study); TtnZr<sub>25</sub>: CaTi<sub>0.75</sub>Zr<sub>0.25</sub>OSiO<sub>4</sub>; RSV<sub>Syn</sub>: Ca<sub>0.85</sub>Na<sub>0.15</sub>Ti<sub>0.7</sub>Nb<sub>0.15</sub>Zr<sub>0.15</sub>OSiO<sub>4</sub>.

*d*<sub>Y</sub>: The displacement of the central atom; ∂<sub>xY</sub>, ∂<sub>yY</sub> and ∂<sub>zY</sub> components of the vector of <sup>Y</sup> atom displacement; Δ<sub>n</sub> Polyhedron bond-length distortion; *v*<sub>n</sub> polyhedron volume distortion; δ<sub>n</sub> bond-angle variance (see text for details). The parameters for P2<sub>1</sub>/a-structured compounds are given in italics.

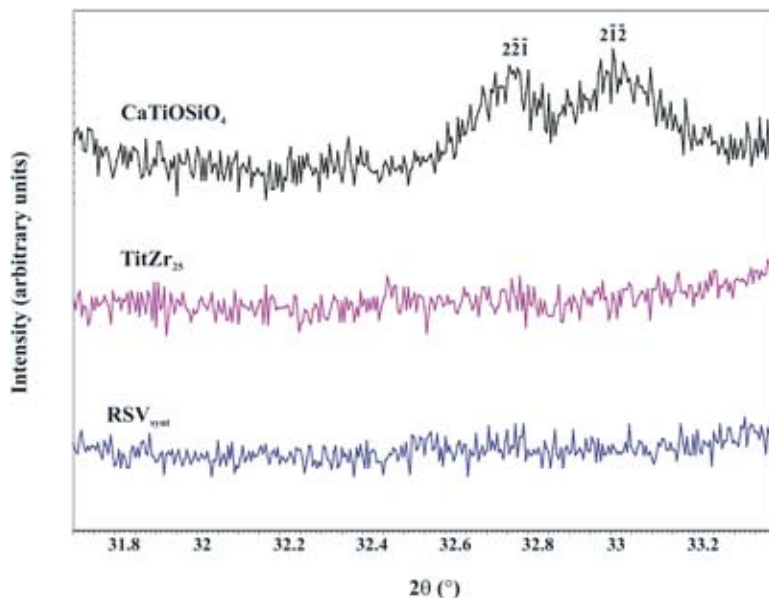


FIG. 5. High-resolution powder X-ray-diffraction patterns over the  $2\theta$  range from 31.7 to 33.4°. The upper pattern (Ttn<sub>Syn</sub>) illustrates the presence of 221 and 222 reflections, which are permitted in space group P2<sub>1</sub>/a. The middle (TtnZr<sub>25</sub>) and lower patterns (RSV<sub>Syn</sub>) do not show any reflections in the  $\sim 33^\circ$   $2\theta$  range, indicating that the Zr- and (Na-Nb-Zr)-bearing variants of titanite adopt space group A2/a.

TABLE 6. POSITIONAL AND THERMAL PARAMETERS OF SYNTHETIC HFSE-RICH TITANITE AT AMBIENT CONDITIONS

	TtnZr <sub>25</sub>					RSV <sub>Syn</sub>				
	<i>x</i>	<i>y</i>	<i>z</i>	SoF	<i>B</i> <sub>iso</sub> [Å <sup>2</sup> ]	<i>x</i>	<i>y</i>	<i>z</i>	SoF	<i>B</i> <sub>iso</sub> [Å <sup>2</sup> ]
<sup>VII</sup> X	¼	0.1680(3)	0	1	1.65(13)	¼	0.1689(4)	0	Ca 0.85(3) Na 0.14(3)	1.48(16)
<sup>VI</sup> Y	½	0	½	Ti 0.76(1) Zr 0.24(1)	0.79(8)	½	0	½	Ti 0.70(1) Nb 0.15(1) Zr 0.15(1)	0.94(3)
<sup>IV</sup> Si	¾	0.1808(5)	0	1	0.30(12)	¾	0.1820(5)	0	1	0.48(13)
O(1)	¾	0.0706(7)	½	1	0.84(9)	¾	0.0669(8)	½	1	0.72(11)
O(2)	0.9099(8)	0.0678(5)	0.1760(8)	1	0.84(9)	0.9108(9)	0.0703(5)	0.1802(9)	1	0.72(11)
O(3)	0.3799(8)	0.2170(5)	0.3920(8)	1	0.84(9)	0.3810(9)	0.2150(6)	0.3987(9)	1	0.72(11)

TtnZr<sub>25</sub>: CaTi<sub>0.75</sub>Zr<sub>0.25</sub>OSiO<sub>4</sub>; RSV<sub>Syn</sub>: Ca<sub>0.85</sub>Na<sub>0.15</sub>Ti<sub>0.70</sub>Nb<sub>0.15</sub>Zr<sub>0.15</sub>OSiO<sub>4</sub>; SoF: refined site-occupancy factors.

TABLE 7. SELECTED BOND-LENGTHS OF SYNTHETIC TITANITE (Å)

	KekTtn*	Ttn <sub>Syn</sub>		TtnZr <sub>25</sub>	RSV <sub>Syn</sub>		KekTtn*	Ttn <sub>Syn</sub>		TtnZr <sub>25</sub>	RSV <sub>Syn</sub>
Ca–O(1)	2.275(1)	2.293(5)	X–O(1)	2.293(7)	2.313(7)	Y–O(1)	1.756(1)	1.755(14)	2× Y–O(1)	1.883(2)	1.876(2)
Ca–O(2)	2.430(1)	2.430(12)	2× X–O(2)	2.425(5)	2.452(5)	Y–O(1')	1.988(1)	1.978(14)	2× Y–O(2)	2.077(5)	2.039(5)
Ca–O(3)	2.409(1)	2.402(12)	2× X–O(3)	2.434(5)	2.445(5)	Y–O(2)	1.991(1)	2.011(15)	2× Y–O(3)	2.093(5)	2.062(5)
Ca–O(4)	2.405(1)	2.394(14)	2× X–O(3')	2.637(6)	2.641(6)	Y–O(3)	1.984(1)	2.007(15)			
Ca–O(4')	2.673(1)	2.752(12)				Y–O(4)	2.012(1)	2.024(13)			
Ca–O(5)	2.423(1)	2.471(15)				Y–O(5)	2.023(1)	2.018(13)			
Ca–O(5')	2.581(1)	2.499(12)				Si–O(2)	1.646(1)	1.619(12)	2× Si–O(2)	1.607(5)	1.607(5)
						Si–O(3)	1.645(1)	1.602(12)	2× Si–O(3)	1.646(7)	1.624(7)
						Si–O(4)	1.647(1)	1.608(16)			
						Si–O(5)	1.651(1)	1.659(16)			

\* Synchrotron-radiation data for CaTiOSiO<sub>4</sub> (Kek *et al.* 1997); Ttn<sub>Syn</sub>: titanite end-member, CaTiOSiO<sub>4</sub> (this study); TtnZr<sub>25</sub>: CaTi<sub>0.75</sub>Zr<sub>0.25</sub>OSiO<sub>4</sub>; RSV<sub>Syn</sub>: Ca<sub>0.85</sub>Na<sub>0.15</sub>Ti<sub>0.70</sub>Nb<sub>0.15</sub>Zr<sub>0.15</sub>OSiO<sub>4</sub>. Parameters for *P*<sub>21</sub>/*a*-structured compounds are given in italics.

Entry of Zr or (Na + Nb) or both into the titanite structure results in larger unit-cell parameters, with the most significant increase in the *a* parameter (along the chains of YO<sub>6</sub> octahedra, Fig. 1). The RSV<sub>Syn</sub> has the greatest unit-cell dimensions *c* and *a*. The TtnZr<sub>25</sub> titanite has the largest *b* unit-cell dimension, greatest β angle, and the largest unit-cell volume (Table 5).

In common with high-pressure – high-temperature titanite and samples of titanite doped with (Al,Fe + F,OH) or (REE + Al), a *P*<sub>21</sub>/*a* → *A*<sub>2</sub>/*a* phase transition

in the titanite varieties doped with Zr and (Na–Nb–Zr) might actually be more complex than revealed by a powder X-ray-diffraction study. This transition might be due to long-range disorder, *i.e.*, antiferroelectric to paraelectric α → β transition (Speer & Gibbs 1976, Ghose *et al.* 1991, Oberti *et al.* 1991, Van Heurk *et al.* 1991, Hughes *et al.* 1997, Kek *et al.* 1997, Troitzsch & Ellis 2002), which is due to the loss of coherency in the displacement of the <sup>VI</sup>Y cations and their “pseudo-centering”. There is also the possibility of a composi-

tionally driven  $\alpha \rightarrow \gamma$  transition, due to the real centering of  $^{VI}Y$  cations. However, conclusions as to the nature of the centering of the  $^{VI}Y$  cations, and discrimination between the  $A2/a$ -structured  $\beta$  and  $\gamma$  polymorphs (Troitzsch & Ellis 2002), are not possible using routine powder X-ray-diffraction techniques.

#### Geometry of the sites

The distortion index  $\Delta_n$  is used to characterize the bond-length distortion in a polyhedron, and defined as  $\Delta_n = 1/n \sum \{(r_i - \bar{r}) / \bar{r}\}^2 \cdot 10^3$ , where  $r_i$  and  $\bar{r}$  are individual and average bond-lengths in the given polyhedron, respectively (Shannon 1976). To characterize deviations from the ideal bond-angles in regular polyhedra ( $90^\circ$  and  $109.47^\circ$  in an ideal octahedron and tetrahedron, respectively), we calculate bond-angle variances,  $\delta_n = \sum [(\theta_i - \theta_{ideal})^2 / (n - 1)]$ , where  $\theta_i$  are the bond angles at  $^{VI}Y$  or  $^{IV}Si$  central atoms (Robinson *et al.* 1971). Polyhedron-volume distortion,  $v_n$ , is calculated using the IVTON software (Balić-Žunić & Vicković 1996) relative to ideal polyhedra with the same coordination numbers and inscribed in a sphere with the radius  $r_s$  (average distance from the relevant centroid to ligands (Makovicky & Balić-Žunić 1998). The calculated indices, plus selected bond-lengths and some framework angles, are listed in Table 5.

#### The tetrahedral site

The samples of synthetic titanite have statistically identical  $\langle Si-O \rangle$  bond lengths (Table 5). The tetrahedron volumes are similar for  $Tn_{Syn}$  and  $TnZr_{25}$ , and slightly smaller for the  $RSV_{Syn}$  sample which, in addition, demonstrates the least amount of bond-length distortion and bond-angle variance in the tetrahedra. Both parameters regularly decrease with the replacement of (Zr,Nb) for Ti in the adjacent octahedral site. The bond-angle variance shown by the tetrahedral site in the  $Tn_{Syn}$  and  $TnZr_{25}$  titanite samples is similar or slightly lower than the value obtained by Troitzsch & Ellis (1999),  $\delta_4 = 17.08$ , for the high-pressure synthetic  $CaAlFSiO_4$  analogue of titanite.

Although variations of bond angles and edges of tetrahedra are typical for most minerals in the titanite group, few unequal Si–O distances have been described to date (Hollabaugh & Foit 1984, Oberti *et al.* 1991, Troitzsch & Ellis 1999). The difference between the shortest and longest Si–O distances in our synthetic Zr- and (Na–Nb–Zr)-bearing samples is between 0.01 and 0.04 Å, and thus similar to that of most samples of titanite.

#### The octahedral site

The kinking of the chains of octahedra is not affected by entry of Na + (Nb,Zr) into the structure, as the pivoting  $Y-O(1)-Y$  angle is similar for  $RSV_{Syn}$  and  $Tn_{Syn}$ .

The single-site  $^{VI}Ti^{4+} \leftrightarrow ^{VI}Zr^{4+}$  substitution alone results in a decrease of the pivoting angle in the synthetic titanite  $TnZr_{25}$  (Table 5).

There is an increase in the mean  $^{VI}Y-O$  distance and  $YO_6$  volume with extent of Zr-for-Ti substitution, from 1.97 Å and 10.10 Å<sup>3</sup> to 2.02 Å and 10.90 Å<sup>3</sup>, in the titanite end-member and the zirconian titanite ( $TnZr_{25}$ ), respectively. The  $RSV_{Syn}$  has a mean  $^{VI}Y-O$  distance (1.99 Å) close to that of the  $CaTiOSiO_4$  end-member, and the  $YO_6$  coordination-polyhedron has an intermediate volume (10.51 Å<sup>3</sup>; Table 5).

The amount of bond-length distortion in the octahedra ( $\Delta_6$ ) is comparable with that in the seven-fold site. Bond-angle variance ( $\delta_6$ ) is less than that in the tetrahedra, whereas the volume distortion of the octahedra ( $v_6$ ) is comparable with that of the tetrahedra, and much less than that of the seven-fold site (Table 5). All the distortion parameters for the octahedral site decrease slightly with replacement of  $^{VI}Ti^{4+}$  by the larger  $^{VI}HFSE$  cations.

The similarity in the extent of distortion of octahedra in the  $P2_1/a$ -structured  $CaTiOSiO_4$  and  $A2/a$ -structured  $RSV_{Syn}$  and  $TnZr_{25}$  implies that the geometrical distortion of the  $YO_6$  coordination polyhedron in titanite studied here is not significantly affected by single-site isovalent or two-site heterovalent substitutions, which result in centering (or pseudocentering) of the  $^{VI}Y$  cations in the HFSE-rich variants of titanite. As is evident from Table 5, the synthetic titanite  $RSV_{Syn}$  has the lowest values, and the  $TnZr_{25}$  titanite has moderate distortions of octahedron bond-lengths, angles, and volume.

#### The $XO_7$ coordination polyhedron

Considerable increase in the mean bond-lengths and volume of the  $XO_7$  polyhedron is observed for the  $RSV_{Syn}$  titanite, in which 15% of positions in the  $XO_7$  site are occupied by  $^{VII}Na^+$ , which is slightly larger than  $^{VII}Ca^{2+}$  (1.10 Å versus 1.06 Å, respectively; Shannon 1976). Single-site substitution of the relatively large  $^{VI}Zr^{4+}$  cation (0.74 Å) affects the  $XO_7$  polyhedron to a much lesser extent (Table 5). As illustrated by the polyhedron bond-length distortion ( $\Delta_7$ ; Table 5), the  $XO_7$  polyhedron in titanite  $TnZr_{25}$  is less distorted than that in the pure titanite end-member. The smallest bond-length distortion of the  $XO_7$  polyhedron is obtained for titanite  $RSV_{Syn}$ . The volume-distortion parameter,  $v_7$ , is not affected by any of the cation-substitution schemes studied here, and is much greater than the indices calculated for  $YO_6$  and  $SiO_4$  polyhedra in all the synthetic variants of titanite.

## CONCLUSIONS

Low-temperature titanite with significant contents of Zr, Al, Fe, and the highest known content of Na and Nb have been recognized in a zeolite vein cutting ultrapotassic rischorrite at Mount Rasvumchorr, Khibina

peralkaline complex. Sodic – niobian – zirconian and zirconian variants of titanite have been synthesized at ambient pressure in air by ceramic techniques and are assumed to be isostructural with (F,OH)-poor natural variants of the Na-, Nb- and Zr-bearing titanite.

The following conclusions are drawn with respect to HFSE-rich varieties of titanite and their (F,OH)-free synthetic analogues:

(i) The highest documented abundances of Nb and Zr in naturally occurring titanite are 16.4 wt.% Nb<sub>2</sub>O<sub>5</sub> (0.25 *apfu* Nb<sup>5+</sup>) and 15.3 wt.% ZrO<sub>2</sub> (0.26 *apfu* Zr<sup>4+</sup>) (Chakhmouradian *et al.* 2003). Entry of Nb into the titanite structure is balanced by up to 3.2 wt.% Na<sub>2</sub>O (0.21 *apfu* Na), this being the highest content of Na observed in natural titanite.

(ii) Crystallization of the synthetic Zr- and (Na–Nb–Zr)-bearing titanite at ambient pressure suggests that their natural analogues might form at low pressure (probably under subvolcanic conditions).

(iii) At the postmagmatic stage of evolution of mantle-derived silica-undersaturated magmas forming peralkaline rocks and their derivatives, titanite may become a sink for Zr and Nb.

(iv) Starting with (F,OH)-free compositions, the consecutive generations of the HFSE-rich titanite in the zeolite vein at Mount Rasvumchorr evolved to compositions deficient in substituting monovalent and trivalent cations. This deficiency is probably compensated by the presence of F<sup>-</sup> and OH<sup>-</sup> replacing the bridging oxygen atoms (O1) in the structure according to the substitution scheme  $^{VII}Na^+ + ^{VI}Nb^{5+} + ^{VI}(Al,Fe)^{3+} + (F,OH)^- \leftrightarrow ^{VII}Ca^{2+} + 2 ^{VI}Ti^{4+} + O(1)^{2-}$ .

(v) Zr- and (Na–Nb–Zr)-bearing variants of titanite, in contrast with the *P2<sub>1/a</sub>*-structured CaTiOSiO<sub>4</sub> end-member, adopt the *A2/a* space group, and consist of irregular *XO<sub>7</sub>* polyhedra and slightly distorted *YO<sub>6</sub>* octahedra and SiO<sub>4</sub> tetrahedra. The antiferroelectric displacement of octahedrally coordinated atoms within the chains of octahedra is disturbed by single-site isovalent substitution at the octahedral site and by complex heterovalent substitution involving the both sevenfold and octahedral sites.

(vi) The volume of the octahedral site increases with substitution of <sup>VI</sup>Zr<sup>4+</sup> and <sup>VI</sup>(Zr<sup>4+</sup>,Nb<sup>5+</sup>) for <sup>VI</sup>Ti<sup>4+</sup>. The additive dimensional effect of (Zr<sub>0.15</sub>Nb<sub>0.15</sub>)<sub>Σ0.30</sub> entry at the <sup>VI</sup>Y site is considerably less than that resulting from Zr<sub>0.25</sub> alone.

(vii) The synthetic analogue of natural titanite from the Rasvumchorr occurrence has the least-distorted coordination polyhedra. The polyhedra in synthetic titanite are moderately distorted, and are similar in this respect to the most zirconian titanite known, and the most strongly distorted polyhedra are found in the CaTiOSiO<sub>4</sub> end-member.

(viii) The weak distortion of the coordination polyhedra comprising the crystal structures of the Zr- and (Na–Nb–Zr)-doped titanite suggests that the capacity of the structure for replacement might exceed 0.25 *apfu*

Zr, and 0.15 *apfu* Na<sup>+</sup> coupled with 0.15 *apfu* Nb<sup>5+</sup> + 0.15 *apfu* Zr<sup>4+</sup>.

(ix) Our data confirm the suitability of titanite for the sequestration of HFSE, as Zr- and (Na–Nb–Zr)-rich variants exist in nature and can readily be synthesized.

#### ACKNOWLEDGEMENTS

This work is supported by the Natural Sciences and Engineering Research Council of Canada and Lakehead University. We are grateful to A. MacKenzie for assistance with the analytical work, and A. Hammond for sample preparation. Special thanks are addressed to Mr. Yu.P. Men'shikov for kind guidance and invaluable supervision in exploring the mineralized areas in the Khibina peralkaline complex. Prof. F.P. Mitrofanov, Director of Geological Institute of Kola Science Center, Russian Academy of Sciences, and Mr. N.I. Bichuk, Director of Murmansk Territorial Committee on Natural Resources, are cordially thanked for permission to undertake field work and support of this study. We thank A. Chakhmouradian, A. Falster, and J. Nizamoff for constructive criticism of an initial version of this manuscript.

#### REFERENCES

- ANGEL, R.J., KUNZ, M., MILETICH, R., WOODLAND, A.B., KOCH, M. & XIROUCHAKIS, D. (1999): High-pressure phase transitions in CaTiOSiO<sub>4</sub> titanite. *Phase Transit.* **68**, 533–543.
- ARZAMASTSEV, A.A. (1994): Unique Paleozoic intrusions of the Kola Peninsula (F.P. Mitrofanov, ed.). Geol. Inst., Kola Sci. Centre, Russ. Acad. Sci., Apatity, Russia.
- BALIĆ-ŽUNIĆ, T. & VICKOVIĆ, I. (1996): IVTON – a program for the calculations of geometrical aspects of crystal structures and some crystal chemical applications. *J. Appl. Crystallogr.* **29**, 305–306.
- ČERNÝ, P., NOVÁK, M. & CHAPMAN, R. (1995): The Al(Nb, Ta)Ti<sub>2</sub> substitution in titanite: the emergence of a new species? *Mineral. Petrol.* **52**, 61–73.
- \_\_\_\_\_ & RIVA DI SANSEVERINO, L. (1972): Comments on crystal chemistry of titanite. *Neues Jahrb. Mineral., Monatsh.*, 97–103.
- CHAKHMOURADIAN, A.R. & MITCHELL, R.H. (1999): Primary, apatitic and deuteric stages in the evolution of accessory Sr, REE, Ba and Nb-mineralization in nepheline-syenite pegmatites at Pegmatite Peak, Bearpaw Mts., Montana. *Mineral. Petrol.* **67**, 85–110.
- \_\_\_\_\_ & \_\_\_\_\_ (2002): New data on pyrochlore and perovskite-group minerals from the Lovozero alkaline complex, Russia. *Eur. J. Mineral.* **14**, 821–836.
- \_\_\_\_\_, REGUIR, E.P. & MITCHELL, R.H. (2003): Titanite in carbonatitic rocks: genetic dualism and geochemical significance. *Per. Mineral.* **72**, Special Issue: Eurocarb, 107–113.

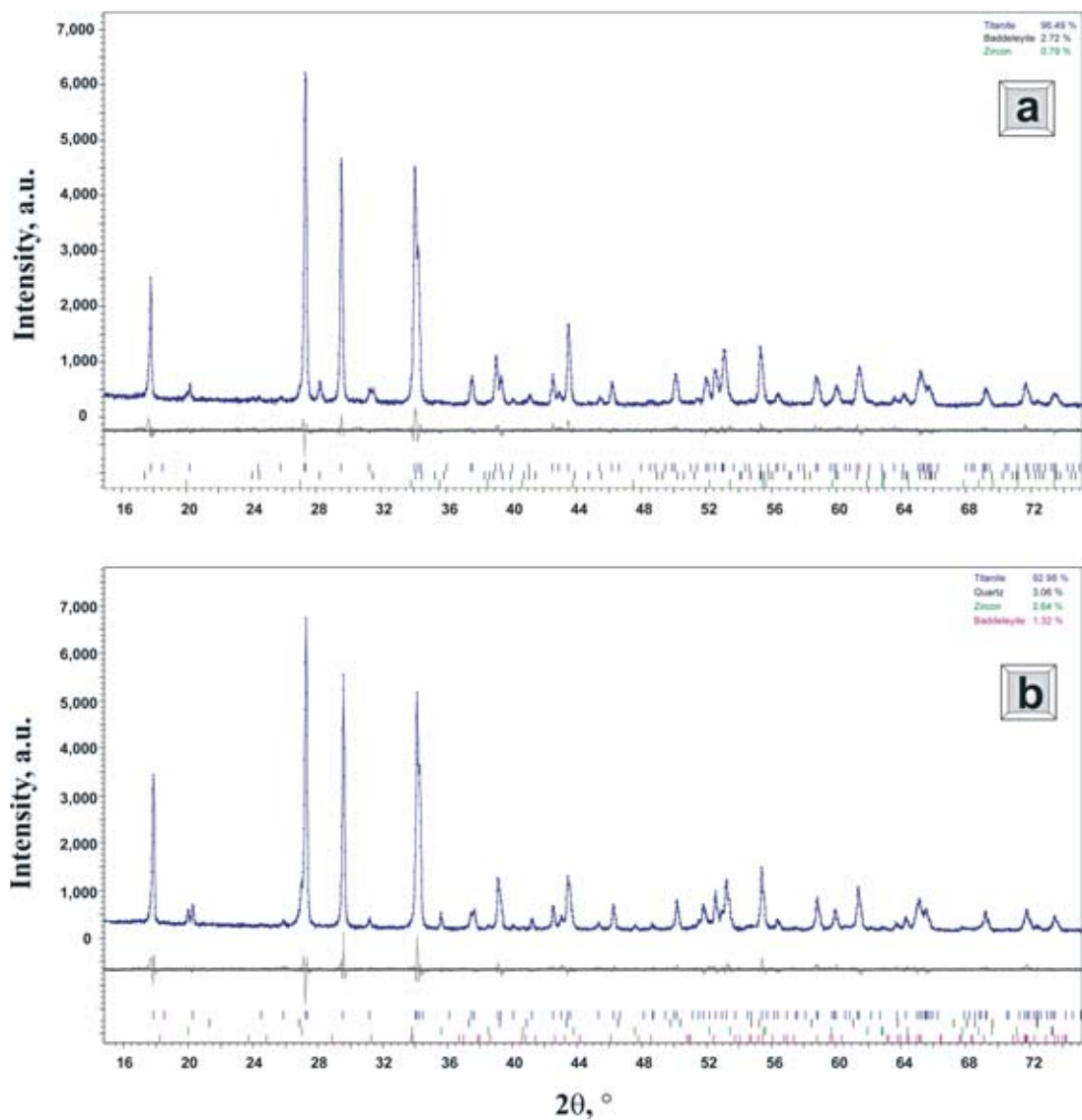


FIG. 6. Rietveld refinement plots (line) of the X-ray powder-diffraction data for synthetic titanite  $TtnZr_{25}$  (a) and  $RSV_{Syn}$  (b) at room temperature (dots). The vertical bars indicate the allowed Bragg reflections. The difference curve between observed and calculated profiles is plotted. For agreement factors, see Table 4.

CHROSCHE, J., BISMAYER, U. & SALJE, E.K.H. (1997): Anti-phase boundaries and phase transitions in titanite: an X-ray diffraction study. *Am. Mineral.* **82**, 677-681.

CLARK, A.M. (1974): A tantalum-rich variety of sphene. *Mineral. Mag.* **39**, 605-607.

DAWSON, J.B., SMITH, J.V. & STEELE, I.M. (1995): Petrology and mineral chemistry of plutonic igneous xenoliths from

the carbonatite volcano, Oldoinyo Lengai, Tanzania. *J. Petrol.* **36**, 797-826.

DELLA VENTURA, G., BELLATRECCIA, F. & WILLIAMS, C.T. (1999): Zr- and LREE-rich titanite from Tre Croci, Vico volcanic complex (Latium, Italy). *Mineral. Mag.* **63**, 123-130.

DOWTY, E. (1999): *Atoms 5.0*. Shape Software, Kingsport, Tennessee 37663, USA.

- GHOSE, S., YOSHIKI, I. & HATCH, D.M. (1991): Paraelectric-antiferroelectric phase transition in titanite,  $\text{CaTiSiO}_5$ . I. A high-temperature X-ray diffraction study of the order parameter and transition mechanism. *Phys. Chem. Minerals* **17**, 591-603.
- GIANETTI, B. & LUHR, J.F. (1983): The white trachytic tuff of Roccamonfina Volcano (Roman region, Italy). *Contrib. Mineral. Petrol.* **84**, 235-252.
- HIGGINS, J.B. & RIBBE, P.H. (1976): The crystal chemistry and space groups of natural and synthetic titanites. *Am. Mineral.* **61**, 878-888.
- HOGARTH, D.D. (1989): Pyrochlore, apatite and amphibole: distinctive minerals in carbonatites. In *Carbonatites: Genesis and Evolution* (K. Bell, ed.). Unwyn Hyman, London, U.K. (105-148).
- HOLLABAUGH, C.L. & FOIT, F.F., Jr. (1984): The crystal structure of an Al-rich titanite from Grisons, Switzerland. *Am. Mineral.* **69**, 725-732.
- HUGHES, J.M., BLOODAXE, E.S., HANCHAR, J.M. & FOORD, E.E. (1997): Incorporation of rare earth elements in titanite: stabilization of the  $A2/a$  dimorph by creation of antiphase boundaries. *Am. Mineral.* **82**, 512-516.
- ISETTI, G. & PENCO, A.M. (1968): La posizione dell'idrogeno ossidrilico nella titanite. *Mineral. Petrogr. Acta* **14**, 115-122.
- IVANOVA, T.N. & ARZAMASTSEV, A.A. (1985): Poikilitic nepheline syenites of the Khibina: geological position, composition, ore prospecting perspectives. In *Petrology and Mineralogy of the Alkaline, Alkaline-Ultramafic and Carbonatite Complexes of the Karelija-Kola Region*. Kola Branch, Akademiya Nauk USSR, Apatity, Russia (13-21; in Russ.).
- KEK, S., AROYO, M., BISMAYER, U., SCHMIDT, C., EICHHORN, K. & KRANE, H.G. (1997): The two-step phase transition of titanite,  $\text{CaTiSiO}_5$ : a synchrotron radiation study. *Z. Kristallogr.* **212**, 9-19.
- KERN, A.A. & COELHO, A.A. (1998): Topas 2.1. *Bruker Axs*. <http://www.bruker-axs.com>
- KHOMYAKOV, A.P. (1995): *Mineralogy of Hyperagpaitic Alkaline Rocks*. Clarendon Press, Oxford, U.K.
- KOZYREVA, L.V., KOROBENIKOV, A.N. & MEN'SHIKOV, YU.P. (1990): New type of the ultrapotassic rocks in Khibina complex. In *New in Mineralogy of Karelija-Kola Region*. Karelija Branch, Akademiya Nauk SSSR, Petrozavodsk, Russia (116-129; in Russ.).
- KULAKOV, A.N. (1981): Titanite mineralization in nepheline syenite massifs, Kola Province. In *Composition of Alkaline Intrusive Complexes, Kola Peninsula*. Kola Branch, Akademiya Nauk SSSR, Apatity, Russia (50-62, in Russ.).
- KUNZ, M., ARLT, T. & STOLZ, J. (2000): In situ powder diffraction study of titanite ( $\text{CaTiOSiO}_4$ ) at high pressure and high temperature. *Am. Mineral.* **85**, 1465-1473.
- \_\_\_\_\_ & BROWN, I.D. (1994): Out-of-center distortions around octahedrally coordinated  $d^0$ -transition metals. *J. Solid State Chem.* **115**, 395-406.
- \_\_\_\_\_, XIROUCHAKIS, D., LINDSLEY, D.H. & HÄUSERMANN, D. (1996): High-pressure phase transition in titanite ( $\text{CaTiOSiO}_4$ ). *Am. Mineral.* **81**, 1527-1530.
- MAKOVICKY, E. & BALIĆ-ŽUNIĆ, T. (1998): New measure of distortion for coordination polyhedra. *Acta Crystallogr.* **B54**, 766-773.
- MALCHEREK, T. (2001): Spontaneous strain in synthetic titanite,  $\text{CaTiOSiO}_4$ . *Mineral. Mag.* **65**, 709-715.
- MEN'SHIKOV, YU.P., POLEZHAeva, L.I. & GANNIBAL, L.F. (1979): Potassian and barian priderites from the Khibina alkaline complex. In *New Data on the Minerals of the Kola Peninsula*. Kola Branch, Akademiya Nauk SSSR, Apatity, Russia (18-24; in Russ.).
- MITCHELL, R.H. & VLADYKIN, N.V. (1993): Rare earth element-bearing tausonite and barium titanates from the Little Murun potassic alkaline complex, Yakutia, Russia. *Mineral. Mag.* **57**, 651-664.
- \_\_\_\_\_, YAKOVENCHUK, V.N., CHAKHMOURADIAN, A.R., BURNS, P.C. & PAKHOMOVSKY, YA.A. (2000): Henrymeyerite, a new hollandite-type Ba-Fe titanate from the Kovdor complex, Russia. *Can. Mineral.* **38**, 617-626.
- MONGIORGI, R. & RIVA DI SANSEVERINO, L. (1968): A reconsideration of the structure of titanite,  $\text{CaTiOSiO}_4$ . *Mineral. Petrogr. Acta* **14**, 123-141.
- OBERTI, R., SMITH, D.C., ROSSI, G. & CAUCIA, F. (1991): The crystal chemistry of high-aluminium titanites. *Eur. J. Mineral.* **3**, 777-792.
- PAUL, B.J., ČERNÝ, P., CHAPMAN, R. & HINTHORNE, J.R. (1981): Niobian titanite from the Huron Claim pegmatite, southeastern Manitoba. *Can. Mineral.* **19**, 549-552.
- PEKOV, I.V. (2001): *Lovozero Massif: History of Investigations, Pegmatites, Minerals*. Ocean Pictures Ltd., Moscow, Russia (in Russ.).
- PERSEIL, E.-A. & SMITH, D.C. (1995): Sb-rich titanite in the manganese concentrations at St. Marcel - Praborna, Aosta Valley, Italy: petrography and crystal chemistry. *Mineral. Mag.* **59**, 717-734.
- PIILONEN, P.C., LALONDE, A.E., McDONALD, A.M., GAULT, R.A. & LARSEN, A.O. (2003): Insights into astrophyllite-group minerals. I. Nomenclature, composition and development of a standardized general formula. *Can. Mineral.* **41**, 1-26.
- REGUIR, E.P., CHAKHMOURADIAN, A.R. & EVDOKIMOV, M.D. (1999): The mineralogy of a unique baratovite- and miserite-bearing quartz - albite - aegirine rock from the Dara-i-Pioz Complex, northern Tajikistan. *Can. Mineral.* **37**, 1369-1384.

- RINGWOOD, A.E., KESSON, S.E., REEVE, K.D., LEVINS, D.M. & RAMM, E.J. (1988): SYNROC. In *Radioactive Waste Forms for the Future* (W. Lutze, & R.C. Ewing, eds.). North-Holland, Amsterdam, The Netherlands (233-334).
- ROBINSON, K., GIBBS, G.V. & RIBBE, P.H. (1971): Quadratic elongation: a quantitative measure of distortion in coordination polyhedra. *Science* **172**, 567-570.
- RUSSELL, J.K., GROAT, L.A. & HALLERAN, A.D. (1994): LREE-rich niobian titanite from Mount Bisson, British Columbia: chemistry and exchange mechanisms. *Can. Mineral.* **32**, 575-587.
- SAHAMA, T.G. (1946): On the chemistry of the mineral titanite. *Bull. Comm. Géol. Finlande* **138**, 88-120.
- SALJE, E., SCHMIDT, C. & BISMAYER, U. (1993): Structural phase transitions in titanite, CaTiSiO<sub>5</sub>: a Raman spectroscopic study. *Phys. Chem. Minerals* **19**, 502-506.
- SEIFERT, W. & KRAMER, W. (2003): Accessory titanite: an important carrier of zirconium in lamprophyres. *Lithos* **71**, 81-98.
- SHANNON, R.D. (1976): Revised effective ionic radii and systematic studies of interatomic distances in halides and chalcogenides. *Acta Crystallogr.* **A32**, 751-767.
- SPEER, J.A. & GIBBS, G.V. (1976): The crystal structure of synthetic titanite, CaTiOSiO<sub>4</sub>, and the domain textures of natural titanites. *Am. Mineral.* **61**, 238-247.
- TAYLOR, M. & BROWN, G.E. (1976): High-temperature structural study of the  $P2_1/a \leftrightarrow A2/a$  phase transition in synthetic titanite, CaTiSiO<sub>5</sub>. *Am. Mineral.* **61**, 435-447.
- TROITZSCH, U. & ELLIS, D. (1999): The synthesis and crystal structural of CaAlFSiO<sub>4</sub>, the Al-F analog of titanite. *Am. Mineral.* **84**, 1162-1169.
- \_\_\_\_\_ & \_\_\_\_\_ (2002): Thermodynamic properties and stability of AlF-bearing titanite CaTiOSiO<sub>4</sub>-CaAlFSiO<sub>4</sub>. *Contrib. Mineral. Petrol.* **142**, 543-563.
- \_\_\_\_\_, \_\_\_\_\_, THOMPSON, J. & FITZGERALD, J. (1999): Crystal structural changes in titanite along the join TiO - AlF. *Eur. J. Mineral.* **11**, 955-965.
- VAN HEURK, C., VAN TENDELOO, G., GHOSE, S. & AMELINCKX, S. (1991): Paraelectric-antiferroelectric phase transition in titanite, CaTiSiO<sub>5</sub>. II. Electron diffraction and electron microscopic studies of the transition dynamics. *Phys. Chem. Minerals* **17**, 604-610.
- VOLOSHIN, A.V., PAKHOMOVSKIY, YA.A., PUSHCHAROVSKIY, D.YU., NADEZHINA, T.N., BAKHCHISARITSEV, A.YU. & KOBYASHEV, YU.S. (1989): Strontio-pyrochlore: composition and structure. *Trudy Mineral. Muzeya, Akad. Nauk SSSR* **36**, 12-24 (in Russ.).
- WOOLLEY, A.R., PLATT, R.G. & EBY, N. (1992): Niobian titanite and eudialyte from the Ilomba nepheline syenite complex, northern Malawi. *Mineral. Mag.* **56**, 428-430.

Received November 20, 2003, revised manuscript accepted February 13, 2004.